VCST Internal Memo

Title: Polarization Sensitivity Measurements for the JPSS J1 VIIRS VisNIR Bands Using the NIST T-SIRCUS
Memo Number: 2015_016
Revision: 01
Date: September 1, 2015
Author: Jeff McIntire
To: Xiaoxiong Xiong and James Butler
Cc: Hassan Oudrari, Kwo-Fu (Vincent) Chiang, Jon Fulbright and Aisheng Wu

---

References

[1] 'VNIR Polarization Sensitivity vs Wavelength using the T-SIRCUS,' Raytheon.
[2] VCST_TECH_REPORT_14_086, 'Preliminary Analysis of T-SIRCUS Polarization Testing,' Jeff McIntire, January 8, 2015.
[3] VCST_TECH_REPORT_15_002, 'Overview of JPSS J1 Polarization Sensitivity Analysis,' Jeff McIntire, David Moyer, and James Young, January 22, 2015.
[4] VCST_TECH_MEMO_2014_002, 'Assessment of FP-11 Polarization Sensitivity for the VIIRS F2 VisNIR Bands,' Jeff McIntire, March 13, 2014.
[5] VCST_TECH_MEMO_2015_002, 'Assessment of FP-11' Polarization Sensitivity for the JPSS J1 VIIRS VisNIR Bands and Comparison to FP-11 Measurements,' Jeff McIntire, February 12, 2015.
[6] 'J1 Polarization Sensitivity Analysis,' E. C. Fest and P. E. King, January 31, 2014.
[7] VIIRS PRD Rev C, 'Joint Polar-orbiting Satellite System (JPSS) Visible Infrared Imaging Radiometer Suite (VIIRS) Performance Requirements Document (PRD).'
[8] VIIRS.10.15.036, 'Polarization Test Source Assembly (PTSA) Calibration and Performance Verification,' Josh Cohen, Dan Tiffany, Eslim Monroy, and Tung Wang, November 13, 2013.
[9] "Facility for spectral irradiance and radiance responsivity calibrations using uniform sources," S. W. Brown, G. P. Eppeldauer, and K. R. Lykke, Appl. Opt. 45(32), 8218–8237 (2006).
[10] Mathematical Methods in the Physical Sciences, Mary L. Boas, John Wiley & Sons, 1985.

1. Introduction

JPSS J1 VIIRS sensor polarization sensitivity was measured for the VisNIR bands M1 and M4 under limited conditions using the NIST T-SIRCUS in post-TVAC testing [1]. Preliminary NASA analysis was reported in [2,3]. This work will provide an overview of the test setup and objectives, analysis methodology, and results as well as a comparison to earlier FP-11 and FP-11' measurements [4,5] and FRED model results [6].

2. Objective

T-SIRCUS measurements were performed under limited conditions for bands M1 and M4 (see Table 1). These observations were compared to the FRED model results to verify the conclusions of the model [6]. The model indicated that the large polarization sensitivity observed in FP-11 and FP-11' was driven by large diattenuation on the edges of the bandpass. The monochromatic T-SIRCUS measurements were integrated across the bandpass in order to compare to the earlier FP-11 and FP-11' measurements. The sensor specifications of interest here is [5]:

V_PRD-12624 – The VIIRS Sensor linear polarization sensitivity of the VIS and NIR bands shall be less than or equal to the values indicated in Table 1 for scan angles less than 45 degrees off Nadir.

The uncertainty of this measurement will be assessed in a separate memo.

2. Test Equipment and Test Configuration

The test setup used during T-SIRCUS testing was nearly identical to that used during FP-11 and FP-11' [8], except that the SIS-100-2 was replaced by a NIST integrating sphere fed by the NIST T-SIRCUS. SIRCUS consists of a series of tunable lasers [9]; for polarization testing, the frequency doubled output from a custom optical parametric oscillator pumped at 532 nm by a Nd:YVO_4 laser was used to produce monochromatic illumination from 397 nm – 424 nm and from 543 nm – 565 nm while a Rhodamine 6G dye laser was used to produce monochromatic illumination from 566 nm to 572 nm. The bandwidth of the optical parametric oscillator was ~0.02 nm in the 400 nm region and ~0.03 nm in the 550 nm region; the bandwidth of the dye laser was also ~0.02 nm.

The T-SIRCUS lasers, via fiber optics, fed a 1 m NIST integrating sphere with a 12 in circular aperture (a radiance monitor was used to track the radiance output from the sphere in real-time). Light exiting this integrating sphere illuminated a sheet polarizer (BVONIR) mounted in a rotating stage, which could be rotated from 0 to 360 degrees. The now polarized light next entered VIIRS telescope aperture. Additional elements were added to the path for supplemental stray light and polarizer efficiency tests. Two stray light tests were conducted: with a "lollipop" obscuration inserted into the path between the integrating sphere and the rotating sheet polarizer, and with the source off. The efficiency of the sheet polarizer was measured by inserting an additional fixed BVONIR polarizer into the path between the rotating polarizer and VIIRS aperture. Various baffling was used to minimize contamination for other sources or paths.

The VIIRS instrument was set to operational mode with the telescope fixed, staring at the source. Bands M1 and M4 were operated in fixed high gain while the Day Night Band (DNB) was in auto gain. VIIRS was mounted on a rotary table, such that the instrument could view the source from different scan angles; for T-SIRCUS testing, VIIRS was positioned to view the source at -8 and +45 degree scan angles.

For all tests (stray light, efficiency, and sensitivity), the polarizer sheet was rotated from 0 to 180 degrees in 15 degree increments. The polarizer sheet dwelled at every angle for a given amount of time (45 or 75 seconds, depending on the test) before transitioning to the next polarizer angle. A shutter on the source was used to provide a dark offset correction; the shutter cycle was 18 or 30 seconds, depending on the test.

A general schematic of the test setup is shown in Figure 1 indicating the placement of the filters and polarizers relative to the path. Figure 2 references the polarizer angle to VIIRS coordinates system including the rotation of the polarizer (in this figure, the view is from VIIRS through the polarizer to the integrating sphere).

3. Methodology

The polarization sensitivity measurements made using T-SIRCUS were analyzed using Fourier analysis [10]. The offset corrected sensor response (dn) at a given wavelength (λ) and polarization angle (α) was modeled as a fourth order Fourier expansion expressed by

$$dn(\alpha,\lambda) = \frac{1}{2}c_0(\lambda) + \sum_{n=1}^{4}\left[c_n(\lambda)\cos(n\alpha) + d_n(\lambda)\sin(n\alpha)\right], \quad (1)$$

where the zeroth and second order Fourier coefficients are defined by the following:

$$\frac{1}{2}c_0(\lambda) = \frac{1}{\pi}\int_0^{\pi} dn(\theta)\partial\theta, \quad (2)$$

$$C_2(\lambda) = \frac{2c_2(\lambda)}{c_0(\lambda)} = \frac{4}{\pi c_0(\lambda)}\int_0^{\pi}\cos(2\theta)dn(\theta)\partial\theta, \quad (3)$$

and

$$D_2(\lambda) = \frac{2d_2(\lambda)}{c_0(\lambda)} = \frac{4}{\pi c_0(\lambda)}\int_0^{\pi}\sin(2\theta)dn(\theta)\partial\theta. \quad (4)$$

Note that the limits on the integrals reflect the extent of the measured polarizer angles, 0 to π. The first, third, and fourth order Fourier coefficients are not considered in this work, other than to state that they are in general subdominant. The Fourier expansion given in Eq. (1) can be rewritten as

$$dn(\alpha,\lambda) = \frac{1}{2}c_0(\lambda)\left[1 + \sum_{n=1}^{4} a_n(\lambda)\cos\left[n\alpha + \delta_n(\lambda)\right]\right], \quad (5)$$

where the degree of linear polarization (DoLP) of the instrument is defined as

$$a_2(\lambda) = \frac{\sqrt{C_2^2(\lambda) + D_2^2(\lambda)}}{\sqrt{a_2^{eff}(\lambda)}} \quad (6)$$

and the phase angle is defined as

$$\delta_2(\lambda) = \frac{1}{2}\tan^{-1}\left[\frac{D_2(\lambda)}{C_2(\lambda)}\right]. \quad (7)$$

Here a_2^{eff} is the polarizer efficiency is the RSS of C_2 and D_2 determined using the cross polarizer data.

In order to compare to the broadband measurements of the polarization sensitivity [4,5], the Fourier analysis described above is integrated over the spectral bandpass, weighted by the broadband input spectrum and spectral transmittance of the sensor, or

$$C_2(B) = \int C_2(\lambda)RSR(\lambda)d\lambda \quad (8)$$

and

$$D_2(B) = \int D_2(\lambda)RSR(\lambda)d\lambda \quad (9)$$

where B indicates a band-dependent quantity. Here RSR denotes the spectral transmittance weighted by the broadband source profile. For band M1, this also includes the transmittance of a long-wave blocking filter, included to reduce the effects of out-of-band leaks in the broadband measurements [4,5]. The Fourier coefficients generated from Eqs. (3) and (4) were resampled to 1 nm from the measured T-SIRCUS wavelengths. Next, the band dependent polarization factor (DoLP) and phase are defined as

$$a_2(B) = \frac{\sqrt{C_2^2(B) + D_2^2(B)}}{\sqrt{a_2^{eff}(B)}} \quad (10)$$

and

$$\delta_2(B) = \frac{1}{2}\tan^{-1}\left[\frac{D_2(B)}{C_2(B)}\right] \quad (11)$$

For clarity in the plotting, here $0 \leq \delta_2(B) < \pi$. The above analysis was also performed on the ray trace model data. The band dependent analysis was only performed on M1 and M4 data.

4. Analysis

The test data acquired during T-SIRCUS polarization testing is listed in Table 1 including the wavelength, target band, HAM side, scan angle, and test type. DNB data was also acquired for M4 wavelengths; however, the analysis of the DNB data is presented in a separate memo. For each wavelength, the polarizer was rotated from 0 to 180 degrees in 15 degree increments. For every polarizer angle measured, the polarizer dwelled for either 45 or 75 seconds (depending on the test). During that time, the shutter on the T-SIRCUS was either open or closed. The time stamps for both the shutter state and polarizer dwell were recorded; these time stamps were matched to VIIRS scan times to determine which scans corresponded to shutter open and which to shutter closed for a given polarizer angle. The data was also screened for wavelength; if the laser wavelength drifted by more than 0.15 nm, the corresponding scans were discarded. Additionally, the data was further screened to eliminate scans during which the shutter state changed within a scan (observed through higher standard deviations over pixels or if the average dn differed significantly from other scans with the same shutter state). Note that for some polarizer angle – wavelength combinations, no valid scans remained after the screening (these cases are listed in Table 3). An example of the data screening is shown in Figure 3; here the first four polarizer angles were measured at a slightly different wavelength, and so they did not lie on the same sinusoid as the rest of the data. Removing those data resulted in a clean two-cycle sinusoid.

VIIRS was in operational day mode during the T-SIRCUS polarization testing. Thus for every scan, 6304 pixels were recorded for each detector in M1 and M4. The average response and standard deviation were determined for each scan and detector, using an outlier rejection. Once the shutter open and closed scans were selected for a given polarizer angle and wavelength, the dn was determined by subtracting the average response of the shutter closed scans from the average response of the shutter open scans.

The thirteen measurements per wavelength (assuming there is valid data for all polarizer angles) were used to determine the Fourier coefficients in Eqs. (2) – (4). For the wavelengths where one or more polarizer angles did not have any valid data, some approximations were made to replace the missing data: data from 0 degrees was used to replace missing data at 180 degrees and vice versa; if one polarizer angle was missing, then a linear interpolation across the interval was made. For the remaining cases, a function fit was used to determine the zeroth and second order Fourier coefficients. The wavelength dependent Fourier coefficients defined in Eqs. (3) and (4) were resampled to 1 nm, then the DoLP and phase were determined from Eqs. (6) and (7).

For the comparisons to the broadband measurements, the resampled Fourier coefficients were integrated over the spectral bandpass, as defined by Eqs. (8) and (9). For M4, the spectral transmittance of VIIRS was convolved with the broadband source profile and renormalized; for M1, the spectral transmittance of VIIRS was convolved with the broadband source profile as well as the transmittance of a long-wave blocking filter and renormalized. Finally, the band dependent DoLP and phase were determined from Eqs. (10) and (11). The average polarizer efficiency for a given band was used in Eq. (10).

5. Ray Tracing Model

A ray trace model developed using the FRED software was constructed for J1 VIIRS following the discovery of larger than expected polarization sensitivity in bands M1 – M4 [6]. The model was used to generate polarized transmittance of the VIIRS optical system using component level measurements and / or models of their behavior. Model polarized transmittance curves were generated for the measured cases listed in Table 1 using a flat spectrum for 12 different input polarization states (corresponding to the measurements of 0 to 165 degrees in increments of 15 degrees). This model data was then processed in the same manner as the measured data using Eqs. (1) – (11).

6. Results

The measured dn for each polarizer angle from stray light (lollipop) testing is shown in Figure 4 for all detectors (at -8 degrees scan angle, HAM side 1); the symbols represent the measured dn. Each detector is represented by a different symbol / color as defined in the legend. There is a small non-zero pedestal of ~0.02 dn at 415 nm and ~0.01 dn at 559 nm; the stray light was considered low enough to be neglected in the following calculations. Figure 5 shows the measured dn for each polarizer angle from efficiency testing shown by the symbols and Fourier series plotted as the solid lines. Figures 6 – 17 graph the polarization sensitivity data for all measurements listed in Table 1. Note that the lines fit the data very well and closely follow a two-cycle oscillation. The second order Fourier components dominate in all cases except where the second order components become very small. The amplitude and phase of the oscillations are observed to vary considerably between detectors for some wavelengths. Note that the missing data in some plots correspond to the list in Table 3.

The DoLP (resampled to 1 nm) is shown in Figures 18 – 22 versus wavelength for the five measured cases listed in Table 1. The upper plot shows the measured DoLP; the middle graph plots the measured DoLP weighted by the measured RSR; and the lower plot graphs the FRED model DoLP weighted by the modeled RSR. Note that here the DoLP becomes larger as one moves away from the center of the bandpass and the DoLP is as large as 80 % (upper plots). However, the wavelength regions with large polarization sensitivity in Figure 18 – 22 correspond to the edges of the spectral bandpass; weighting the DoLP by the spectral transmittance of the system, as shown in the middle plots, indicates that the DoLP increases on both sides of the bandpass, and then decreases in the middle. This conclusion holds for both M1 and M4. For the M4 case, the DoLP oscillates in the center of the bandpass; the minimums in DoLP correspond to phase angle shifts in the polarization sensitivity. The corresponding ray trace model results are shown in lower plots of Figures 18 – 22. Note that the model and measurements agree in the general shape and characteristics of the DoLP versus wavelength. For M1, the modeled bandpass is slightly wider than the measurement; for M4, the modeled bandpass is also wider and the phase angle shifts that occur in the center of the bandpass were not captured in the model.

Figures 23 – 27 plot the phase angle versus wavelength for the five measured cases listed in Table 1 (upper plot) along with the model results (lower plot). For both M1 cases, the model and measurements agree well in terms of the phase angle behavior; in contrast, the M4 measurements show a phase angle shift in the center of the bandpass that does not appear in the model results. This shift occurs when the second order Fourier coefficient C_2 passes though zero and corresponds to the minima in the DoLP that were observed in the middle of the M4 bandpass.

The band dependent DoLP and phase angles are shown for all measured cases in Figures 28, 30, 32, 34, and 36 (upper and lower plots, respectively). The black '+'s indicate the T-SIRUCS measurements, the red '*'s denote the broadband FP-11 measurements, and the blue '◊'s refer to the model results. The differences between the FP-11 measurements and T-SIRCUS and model results are shown in the corresponding Figures 29, 31, 33, 35, and 37 (red '*'s denote the difference between FP-11 and T-SIRCUS, and the blue '◊'s refer to the difference between FP-11 and the model). In general, the T-SIRCUS results agree reasonably well with the broadband FP-11 measurements. There are differences in the DoLP for both the M1 and M4 cases of up to ~0.5 % compared to the broadband measurements. Note that the M1 and M4 bandpasses were not critically sampled (the laser bandpass was much less than 1 nm). Model differences with measurements are up to ~1.0 % for M1, and larger for M4 (as high as 1.5 %); for M4, the detector dependence was not captured well by the model. This may result from the model not predicting the phase angle shifts occurring in the center of the M4 bandpass. The phase angles are very similar for the M1 cases; however, for M4, the phase angle differences between T-SIRCUS and broadband measurements were larger for higher number detectors, up to ~14 degrees (model disagreement is up to ~12 degrees). Note that model results were available for only one HAM side (most likely HAM 0), which could explain some of the differences.

7. Summary

T-SIRCUS polarization sensitivity testing was performed under ambient conditions for JPSS J1 VIIRS sensor. Analysis showed the following:

- Measurements confirmed the conclusions of ray tracing model in that larger diattenuation on both edges of the bandpass was driving the observed large polarization sensitivity in broadband testing. Phase shifts in the center of the bandpass observed in T-SIRCUS testing were not well reproduced by the model.
- The band dependent polarization sensitivities derived from T-SIRCUS testing compared favorably with the broadband measurements (to within 0.5 % in DoLP and to within 14 degrees in phase angle). Comparisons to the model showed larger differences (up to 1.5 % in DoLP and 12 degrees in phase angle). In particular, the detector to detector behavior in M4 was not well reproduced by the model.

Table 1: T-SIRCUS polarization measurements performed as a function of wavelength, HAM side, scan angle, and test type (stray light, polarizer efficiency, or polarization sensitivity). Wavelengths were rounded to the nearest nm.

Test Type	HAM side	Scan Angle [degrees]	Target Band	Wavelengths [nm]
Stray Light – Dark	1	-8		NA
Stray Light – Lollipop	1	-8	M1 M4	415 559
Polarizer Efficiency	1	-8	M1 M4	401, 412, 420 559
Polarization Sensitivity	1	-8	M1	397, 400, 402, 404, 406, 408, 410, 413, 415, 417, 419, 421, 424
Polarization Sensitivity	1	+45	M1	397, 399, 402, 404, 406, 408, 410, 413, 415, 417, 419, 421, 424
Polarization Sensitivity	1	-8	M4	543, 546, 547, 548, 550, 552, 553, 555, 556, 558, 560, 561, 562, 564, 567, 569, 572
Polarization Sensitivity	0	-8	M4	543, 545, 547, 548, 550, 553, 556, 559, 562, 564, 566, 569, 572
Polarization Sensitivity	1	+45	M4	543, 545, 547, 549, 551, 552, 553, 554, 556, 558, 559, 561, 562, 564, 567, 569, 572

Table 2: Specified maximum polarization sensitivity [7]

Band	Sensitivity [%]
I2, M1, M7	3
I1, M2, M3, M4, M5, M6	2.5

Table 3: Test and wavelengths for which data screening eliminated all scans for the listed polarization angles

Test	Wavelength [nm]	Polarizer Angles
M1 Efficiency	413	0
	421	0, 15, 30, 45, 60
M1, HAM A, -8	400	0
	404	15
	415	105, 120, 135, 150, 165
	419	0, 15, 30, 45
	424	150, 165
M1, HAM A, +45	408	180
	419	0, 15, 30
M4, HAM A, -8	546	150
	550	0, 15, 30
	560	105, 120, 135
	561	75, 90
M4, HAM A, +45	543	0
	552	150, 165
	554	0, 15
	556	0, 15, 30, 45

Figure 1: Schematic of the polarization sensitivity test setup

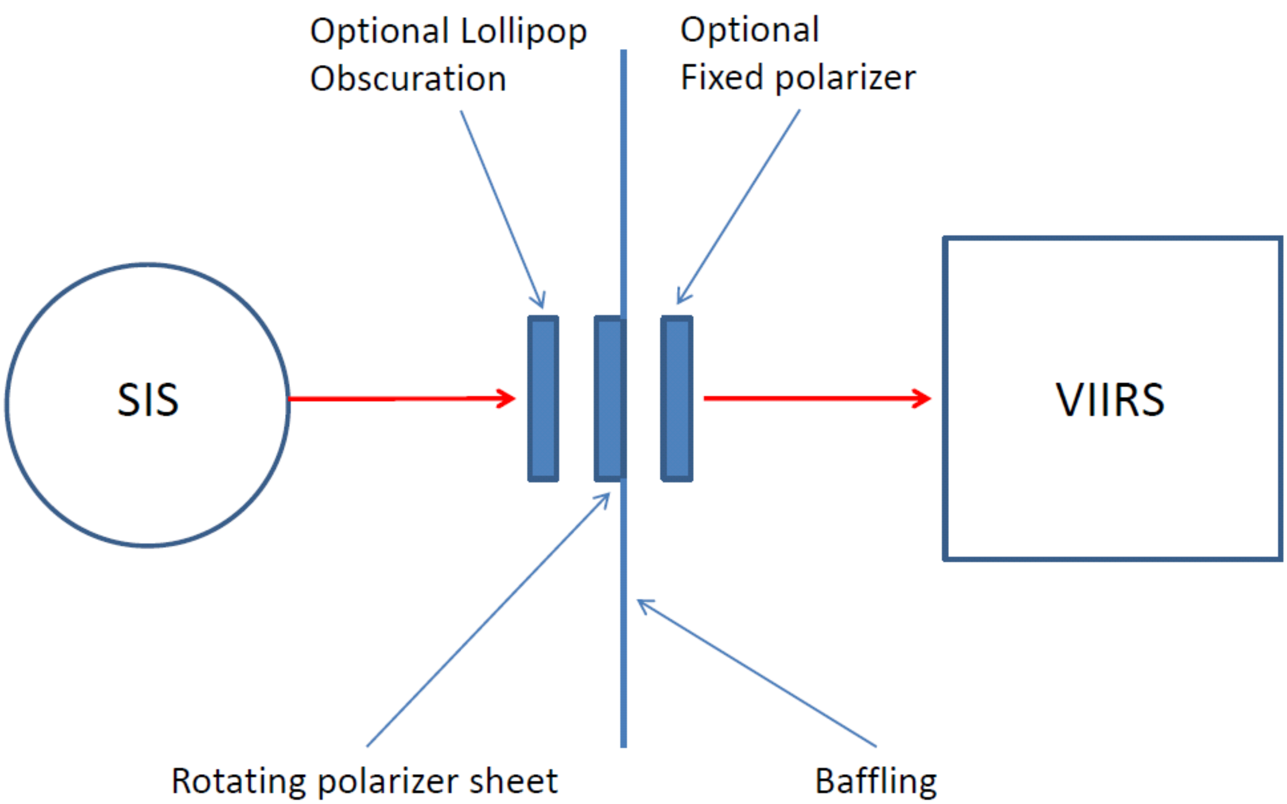

Figure 2: Schematic of the view of BVONIR polarizer from VIIRS with VIIRS coordinate system

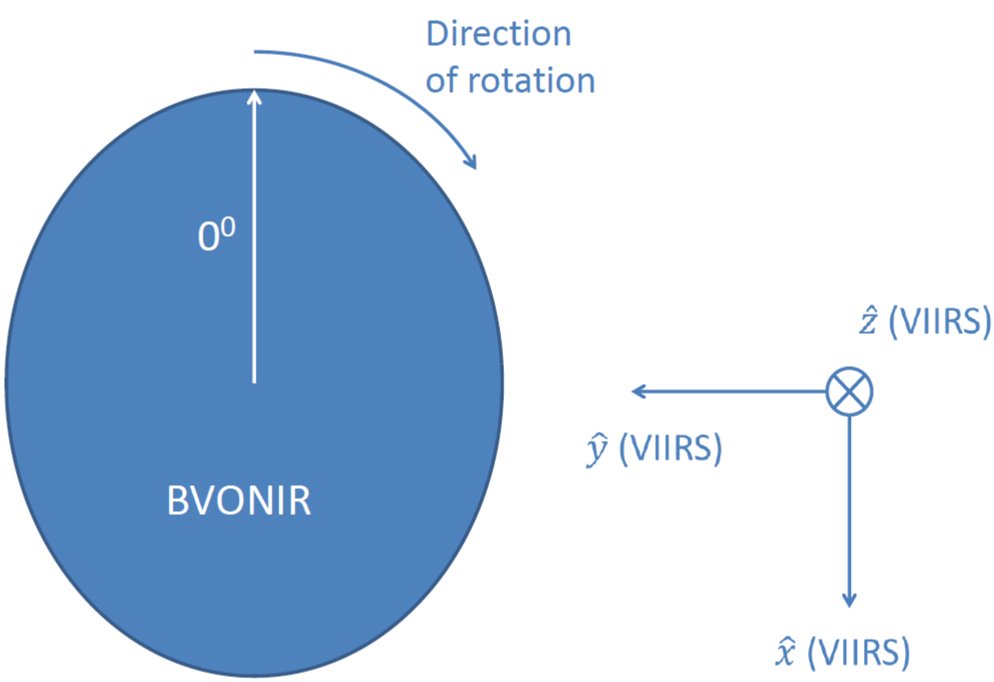

Figure 3: Example of all data without data screening (upper plot) and with screening (lower plot) using M1 data (45 degrees, HAM A, 419 nm).

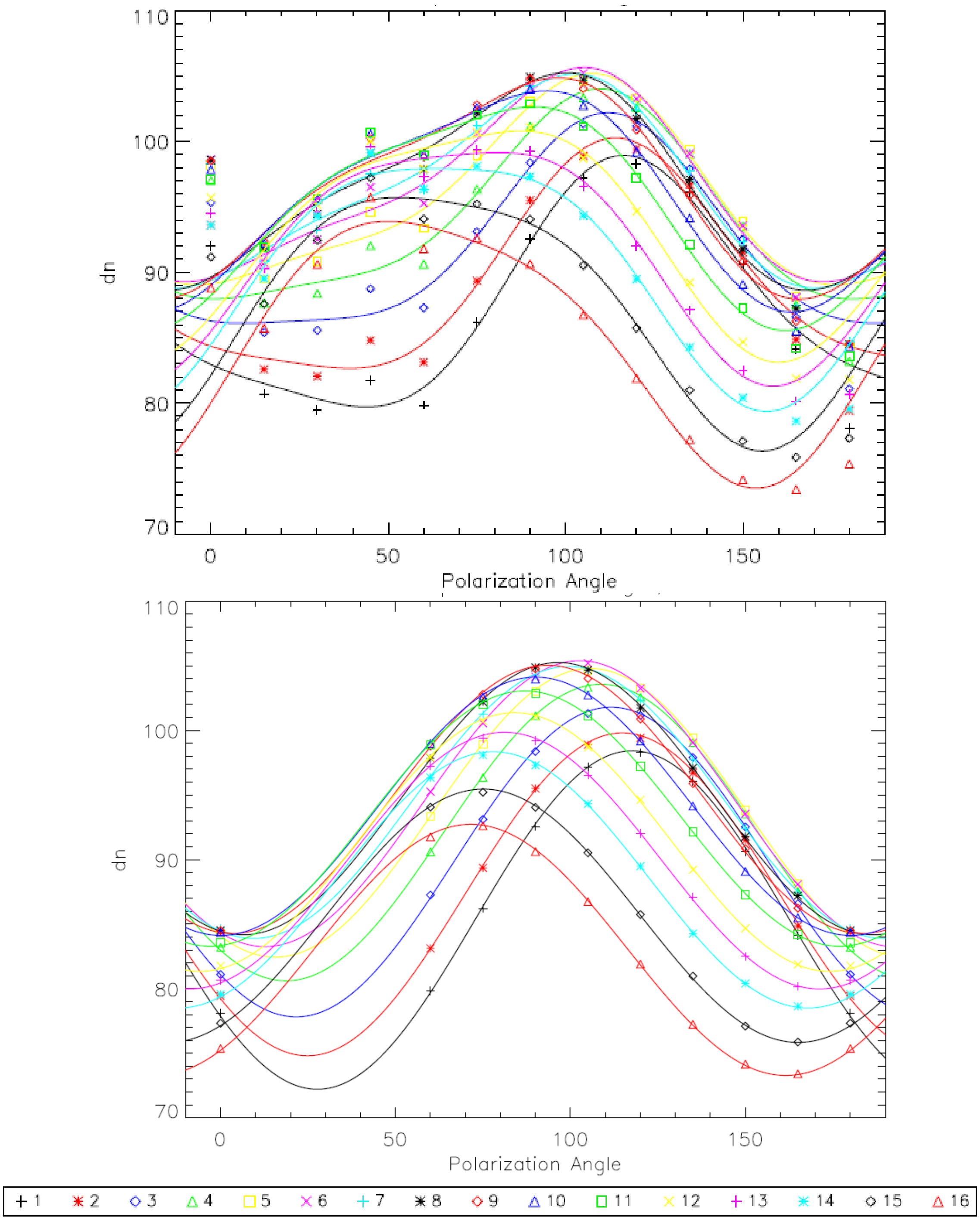

Figure 4: dn versus polarization angle [degrees] for the lollipop tests, at -8 degrees scan angle, HAM 1 at various wavelengths

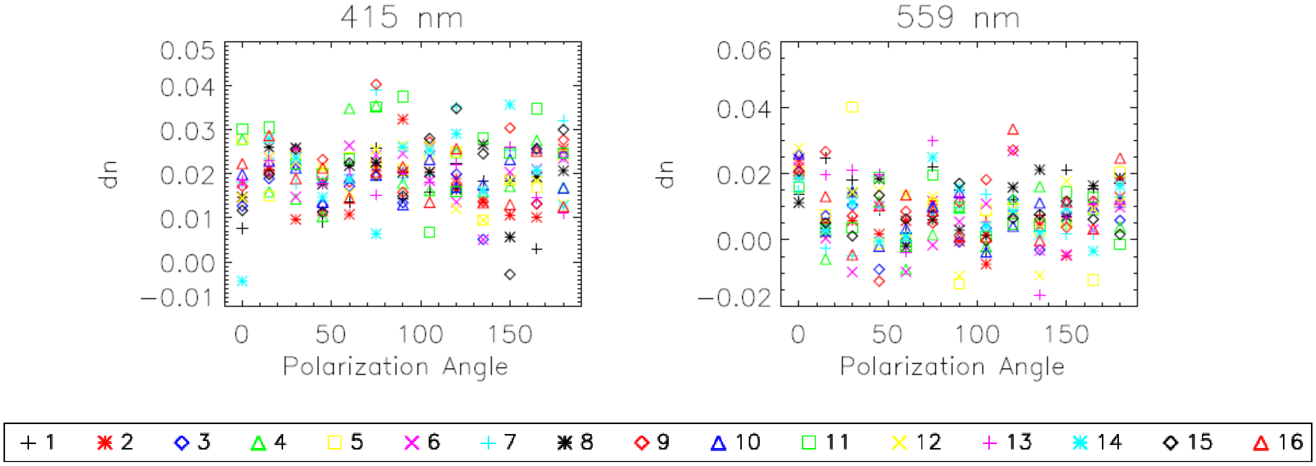

Figure 5: dn versus polarization angle [degrees] for the efficiency tests, at -8 degrees scan angle, HAM 1 at various wavelengths

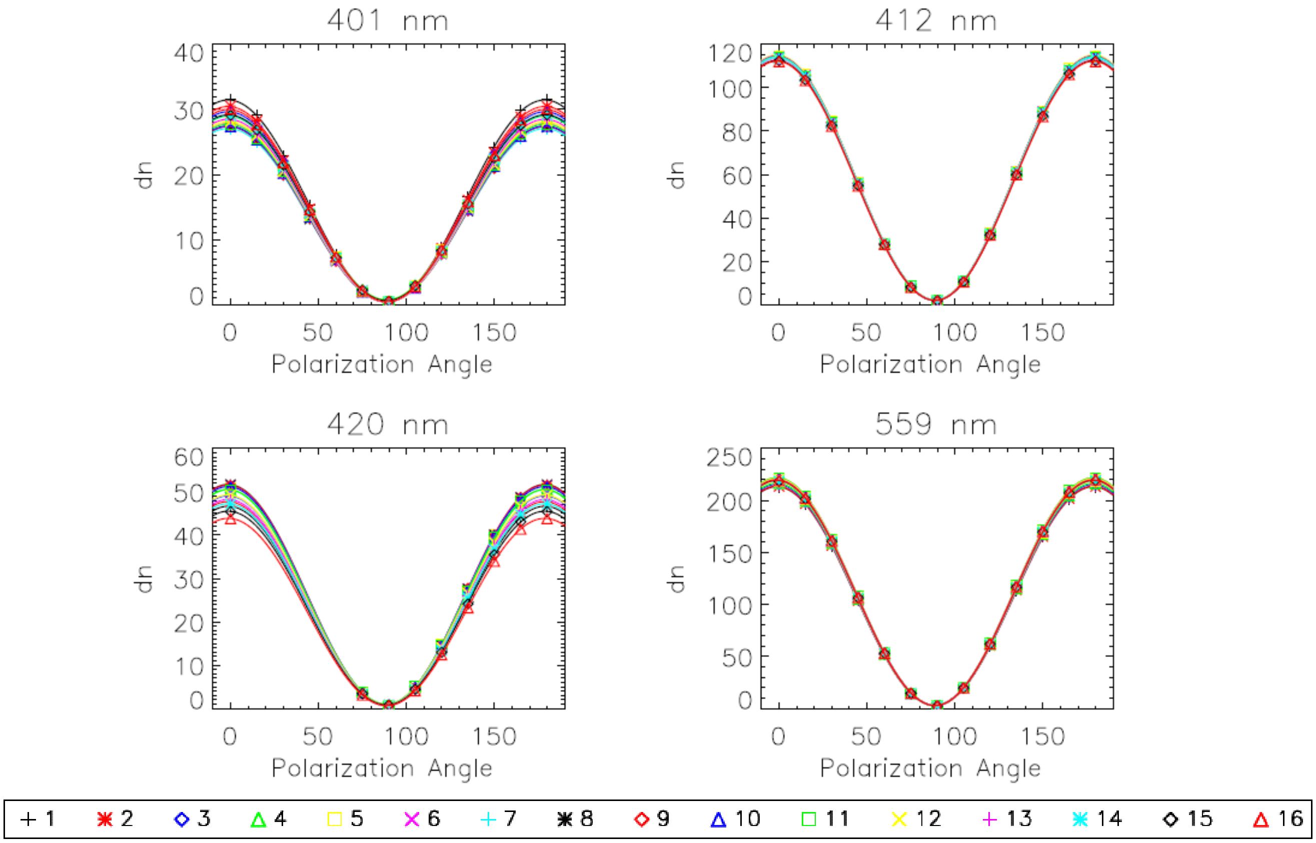

Figure 6: dn versus polarization angle [degrees] for band M1, at -8 degrees scan angle, HAM 1 at various wavelengths

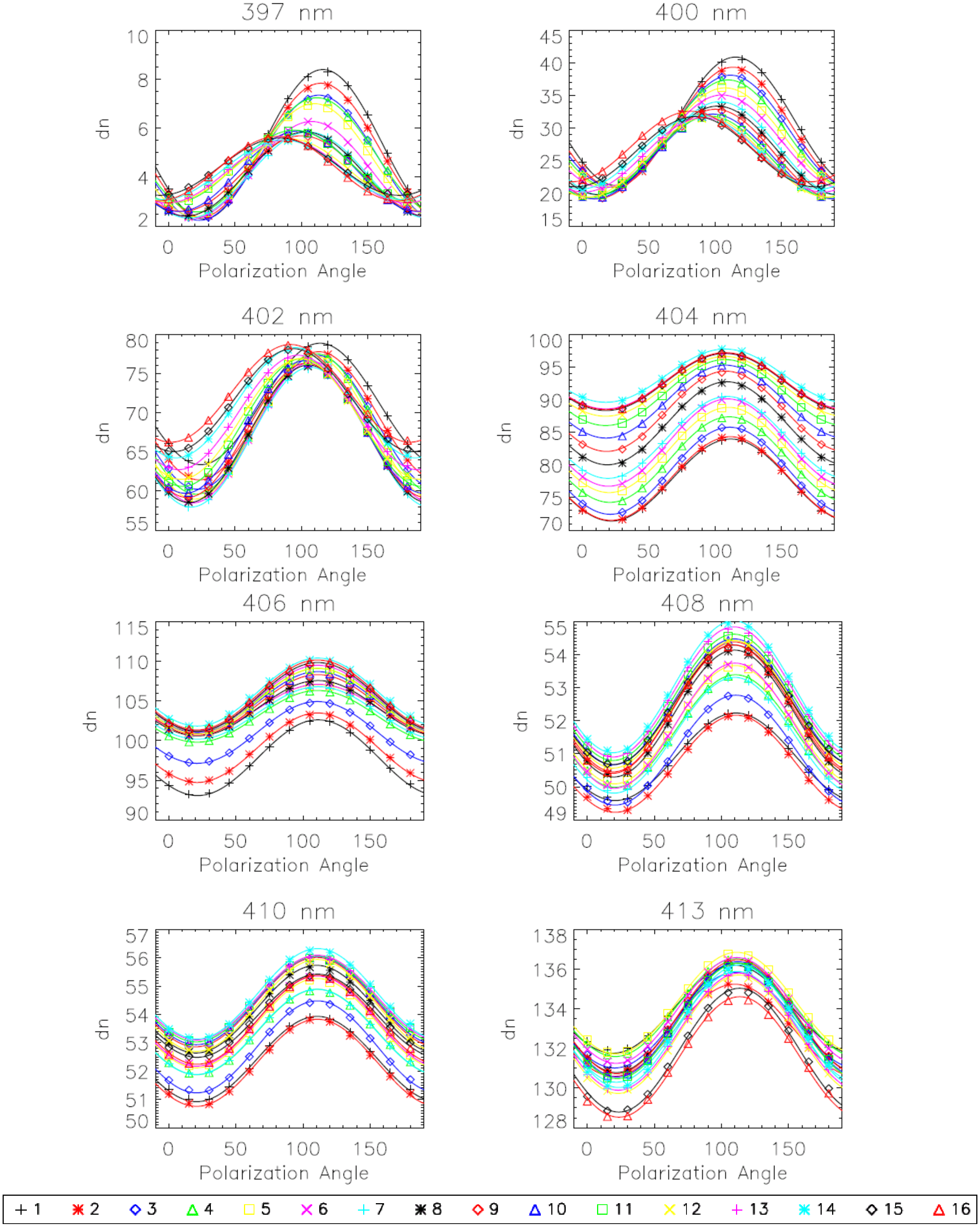

Figure 7: dn versus polarization angle [degrees] for band M1, at -8 degrees scan angle, HAM 1 at various wavelengths

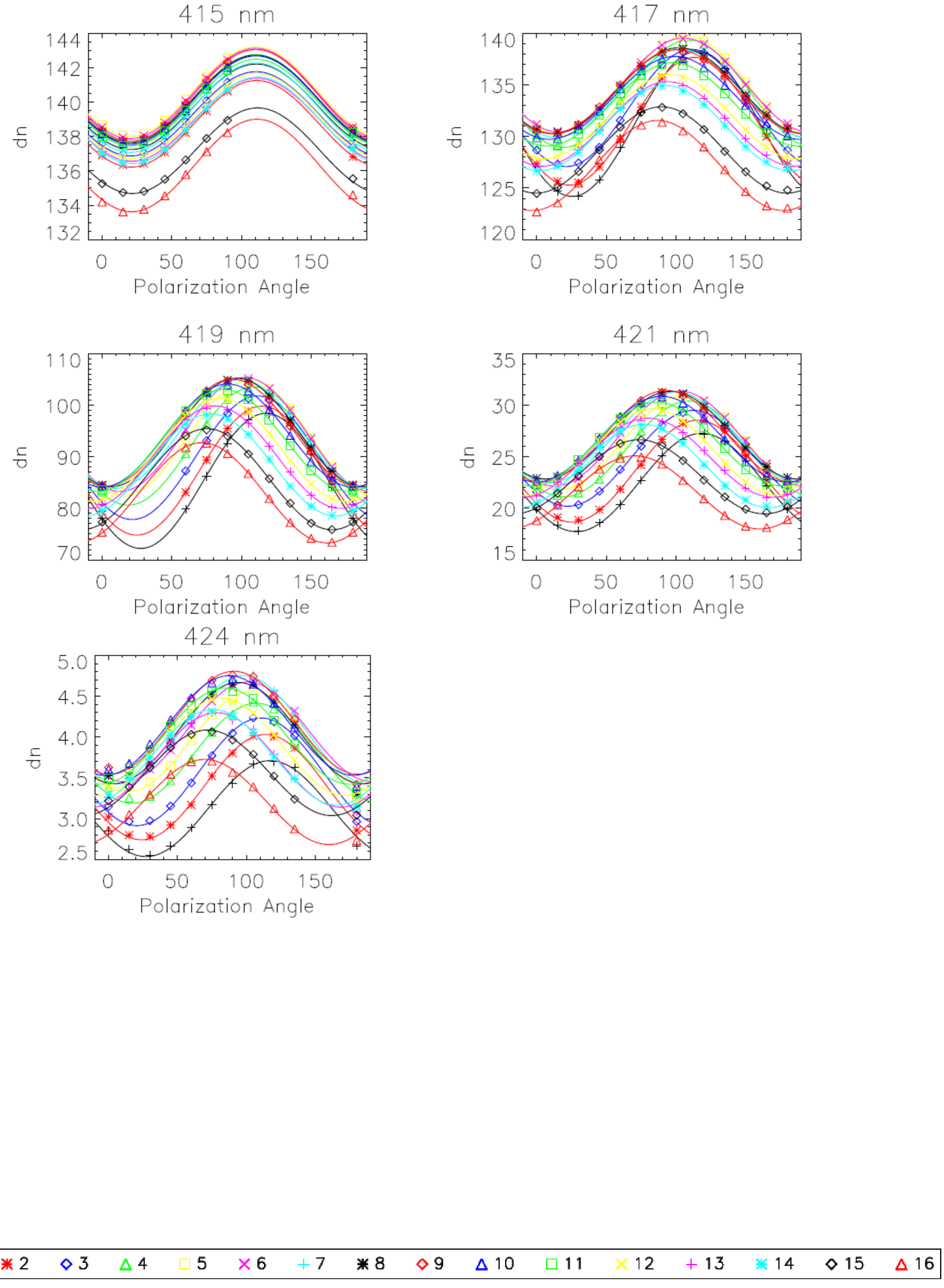

Figure 8: dn versus polarization angle [degrees] for band M1, at +45 degrees scan angle, HAM 1 at various wavelengths

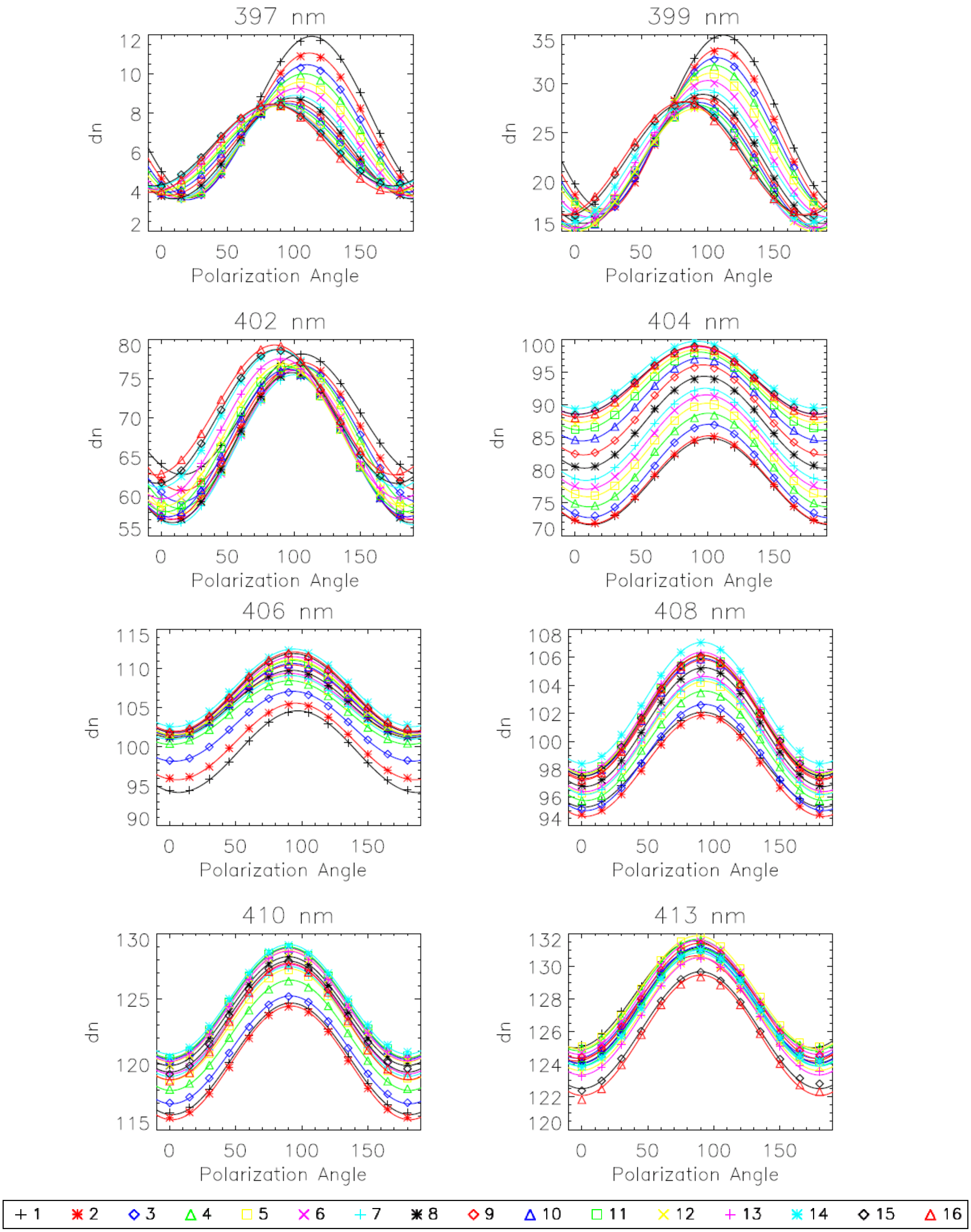

Figure 9: dn versus polarization angle [degrees] for band M1, at +45 degrees scan angle, HAM 1 at various wavelengths

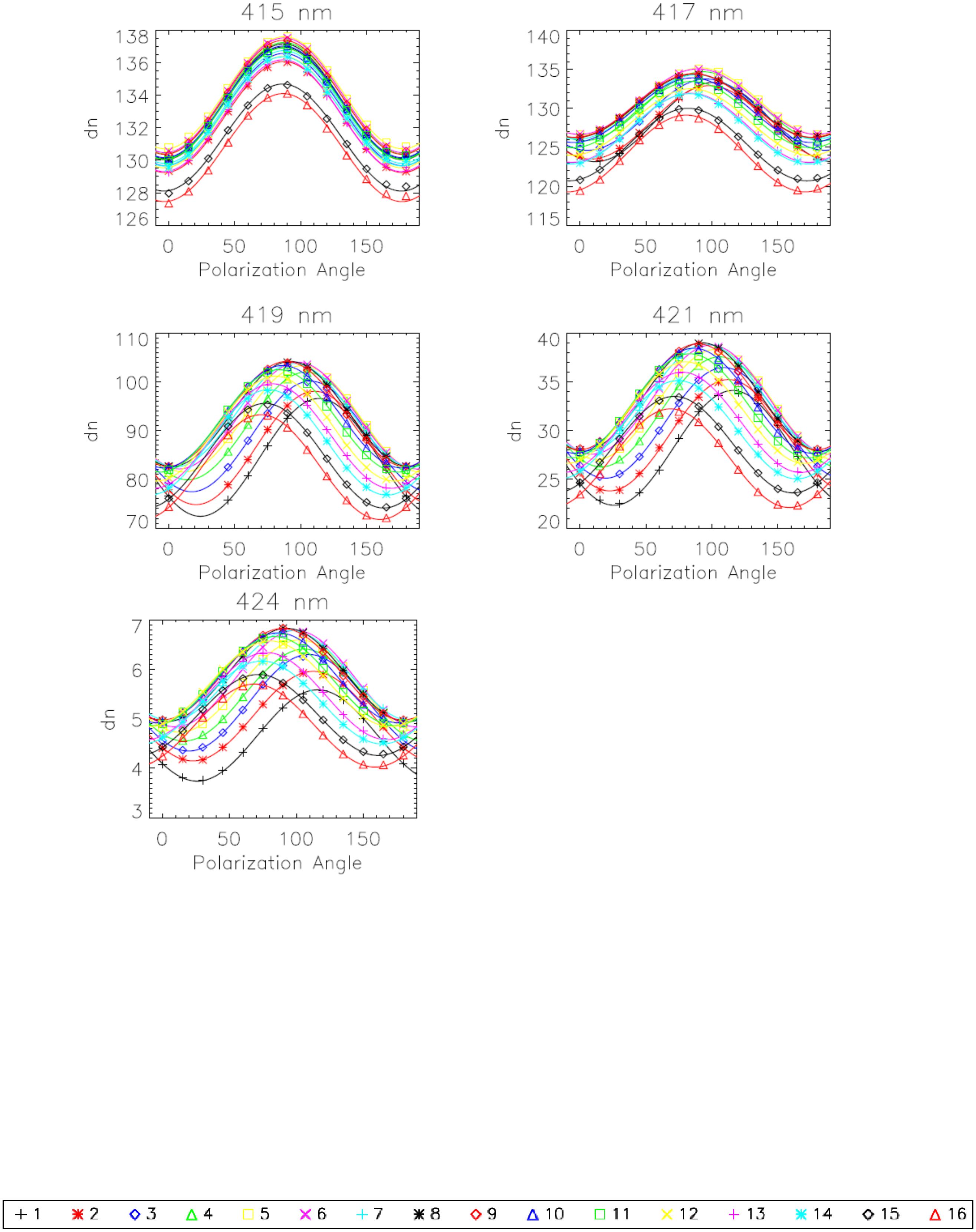

Figure 10: dn versus polarization angle [degrees] for band M4, at -8 degrees scan angle, HAM 1 at various wavelengths

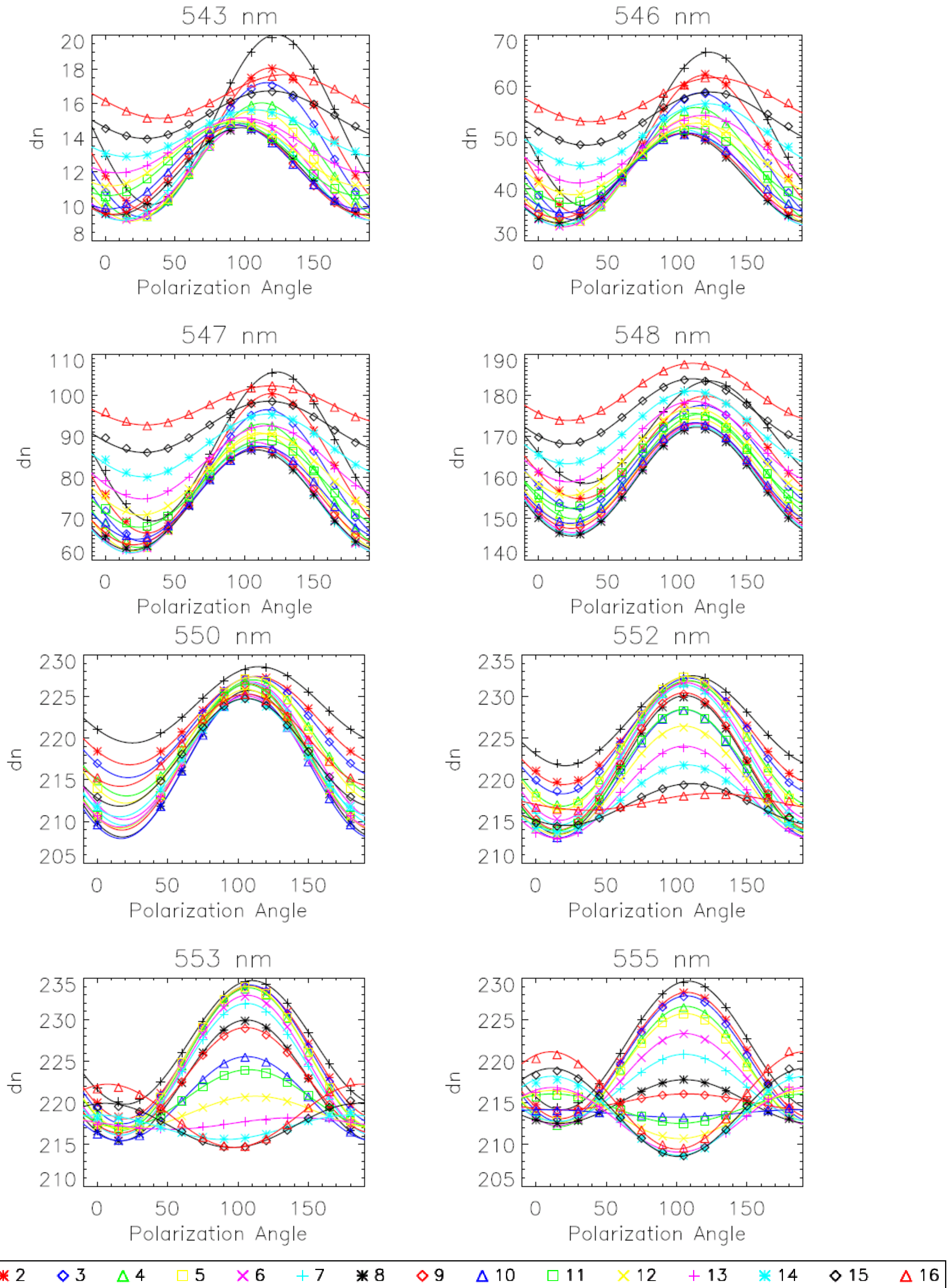

Figure 11: dn versus polarization angle [degrees] for band M4, at -8 degrees scan angle, HAM 1 at various wavelengths

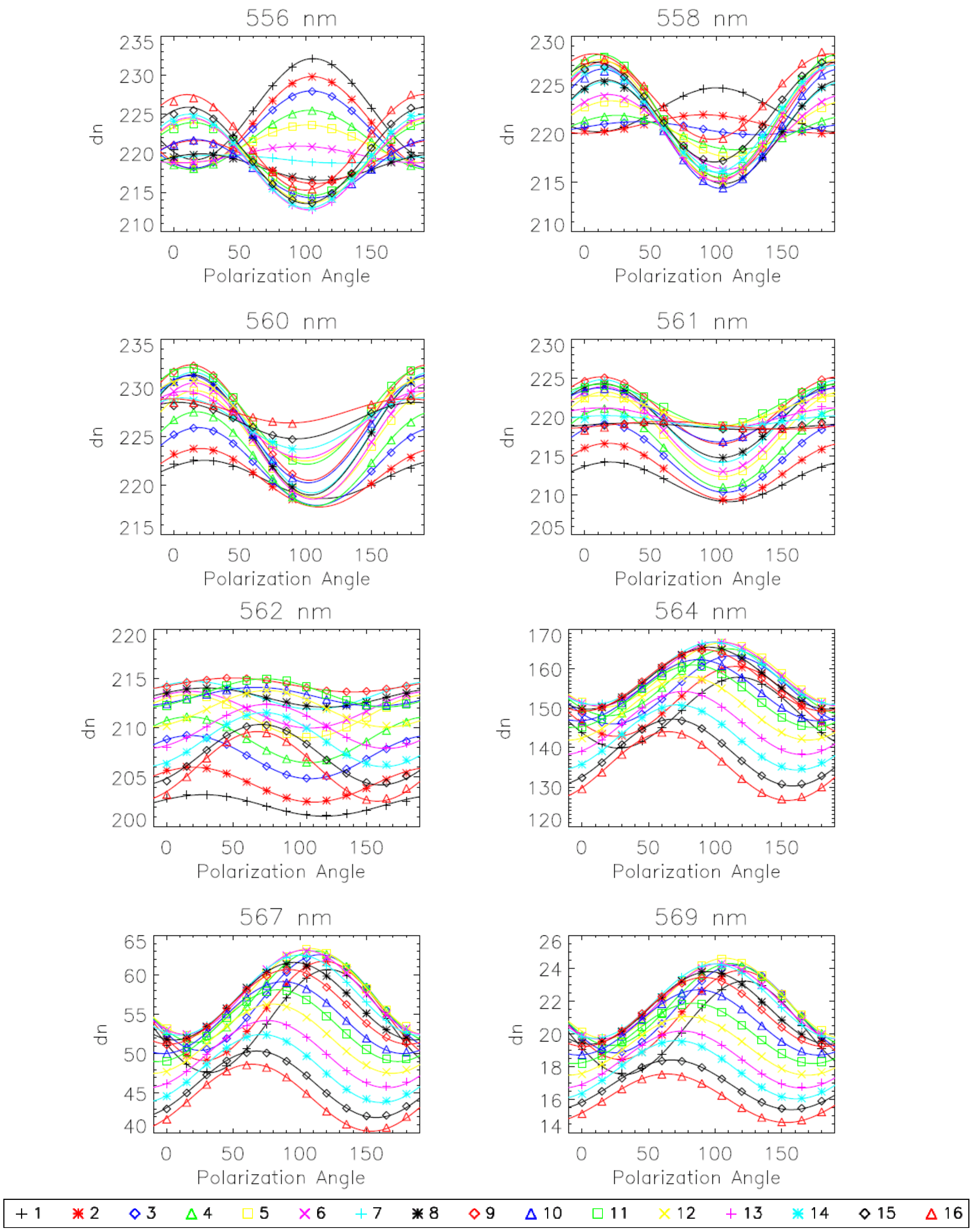

Figure 12: dn versus polarization angle [degrees] for band M1, at -8 degrees scan angle, HAM 1 at various wavelengths

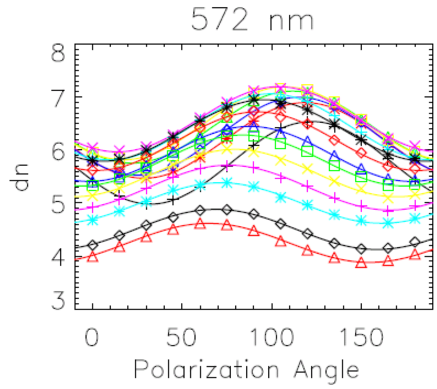

Figure 13: dn versus polarization angle [degrees] for band M4, at -8 degrees scan angle, HAM 0 at various wavelengths

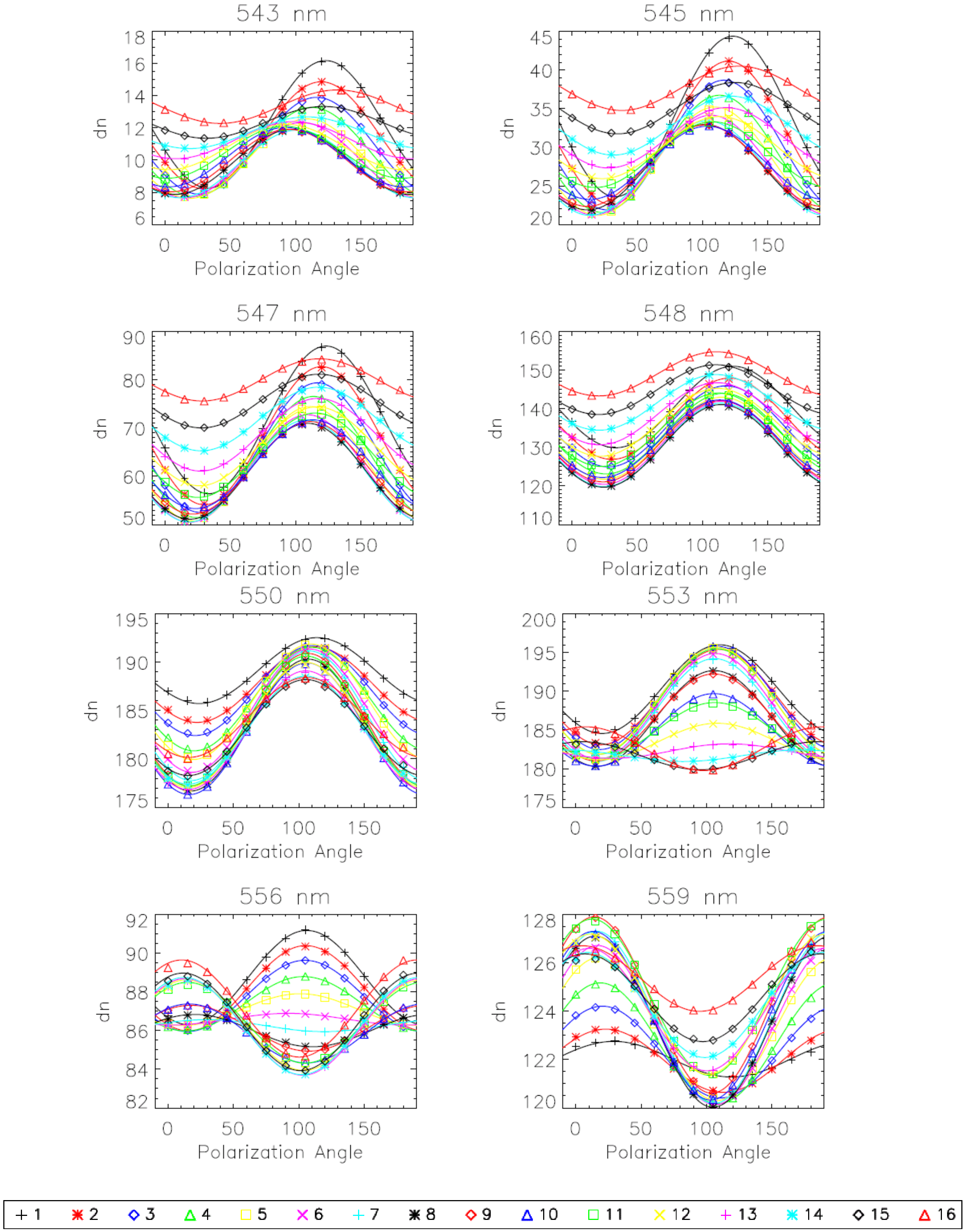

Figure 14: dn versus polarization angle [degrees] for band M4, at -8 degrees scan angle, HAM 0 at various wavelengths

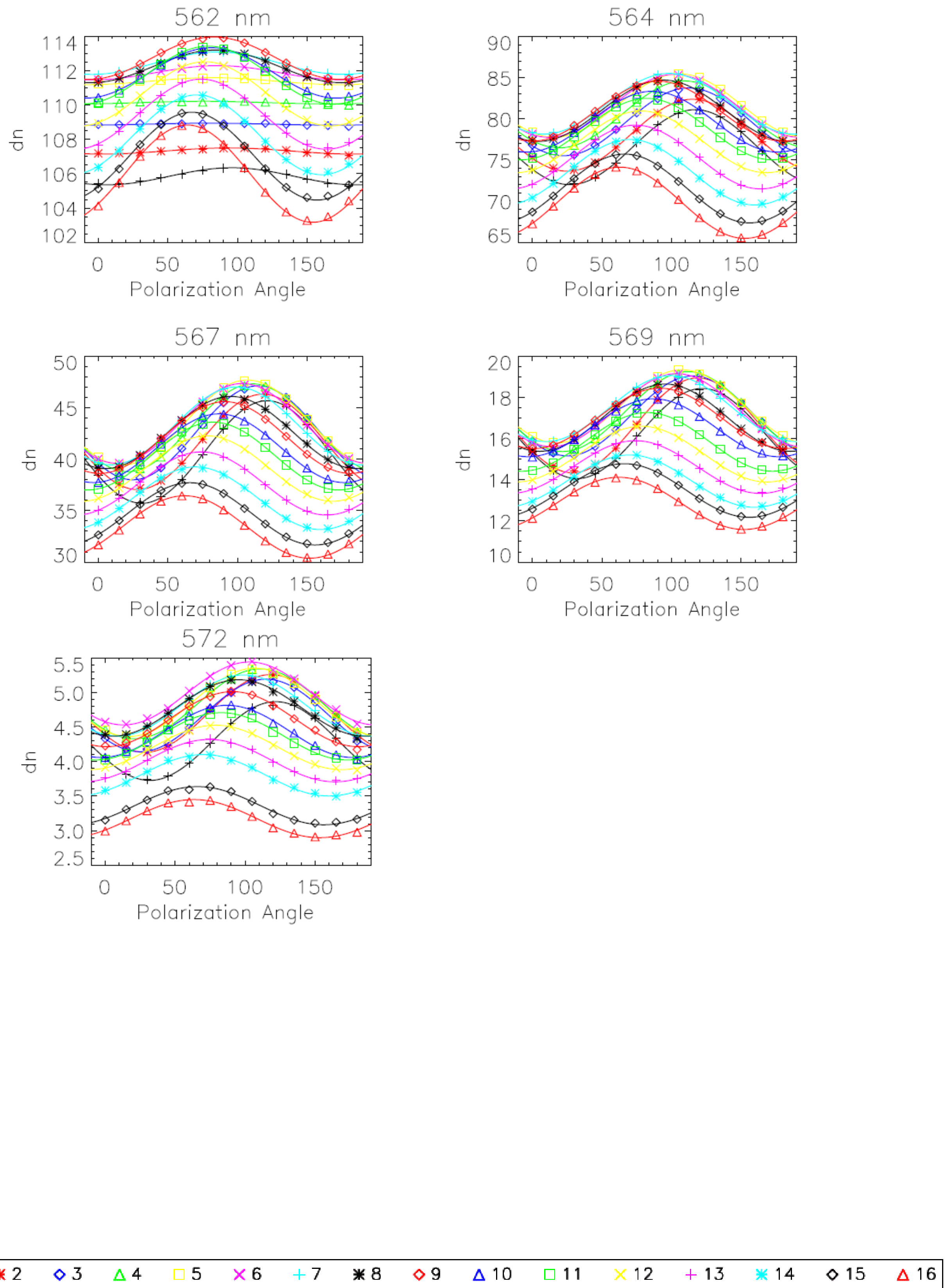

Figure 15: dn versus polarization angle [degrees] for band M4, at +45 degrees scan angle, HAM 1 at various wavelengths

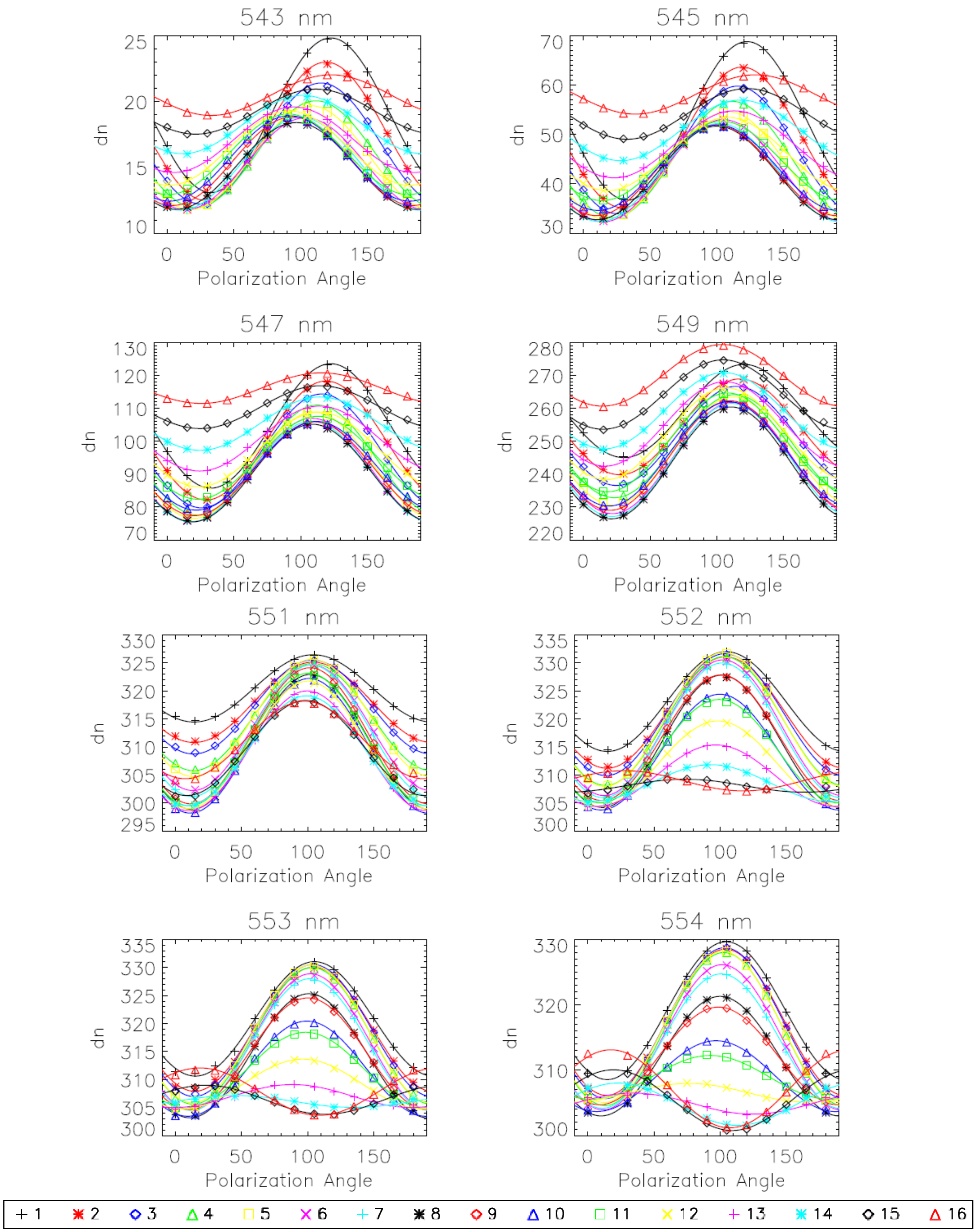

Figure 16: dn versus polarization angle [degrees] for band M4, at +45 degrees scan angle, HAM 1 at various wavelengths

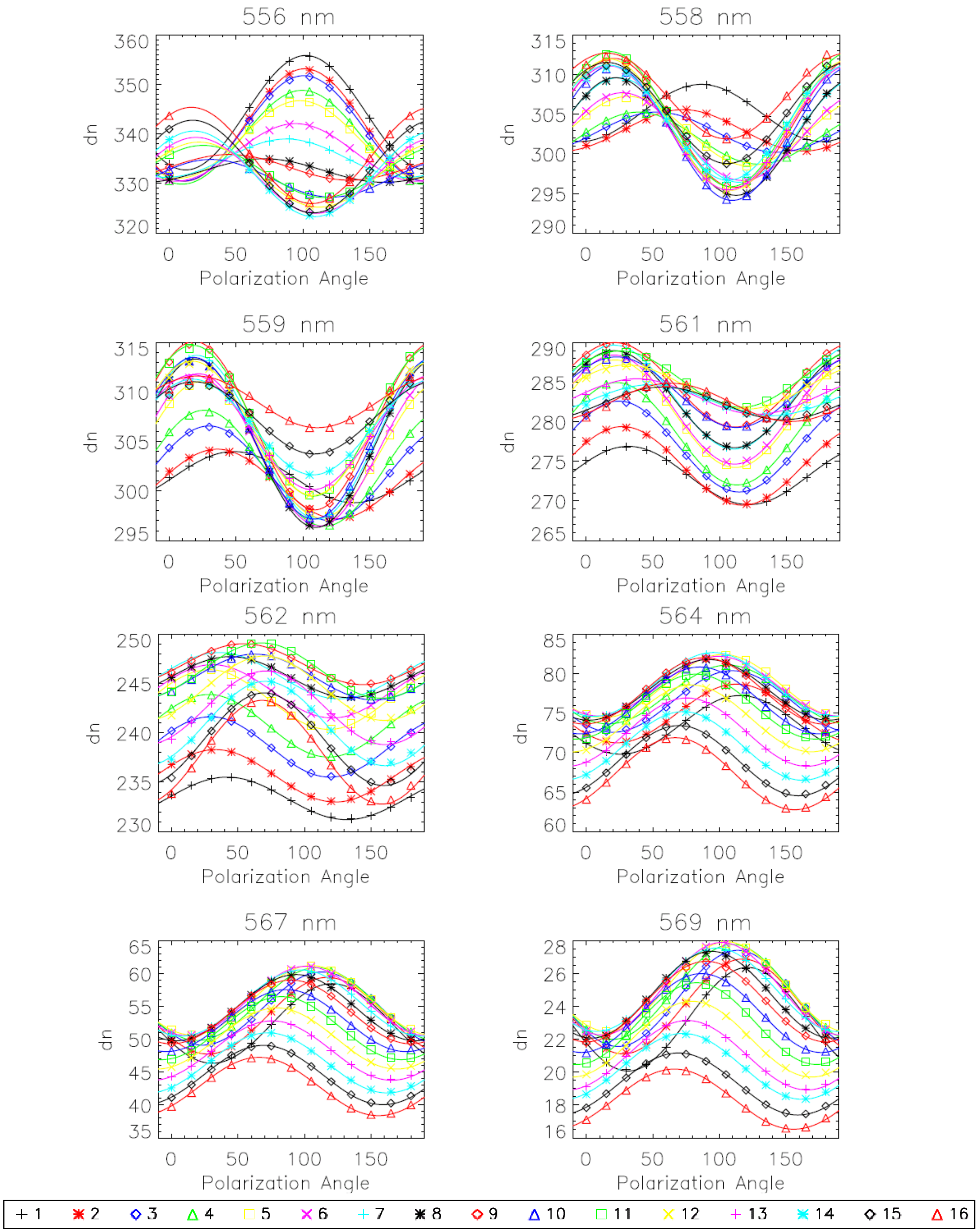

Figure 17: dn versus polarization angle [degrees] for band M4, at +45 degrees scan angle, HAM 1 at various wavelengths

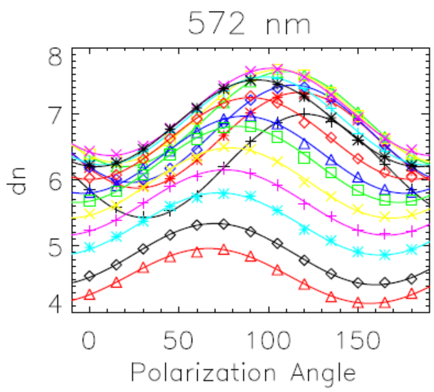

Figure 18: DoLP [%] versus wavelength [nm] for band M1, at -8 degrees scan angle, HAM 1 (unweighted, weighted, and weighted model)

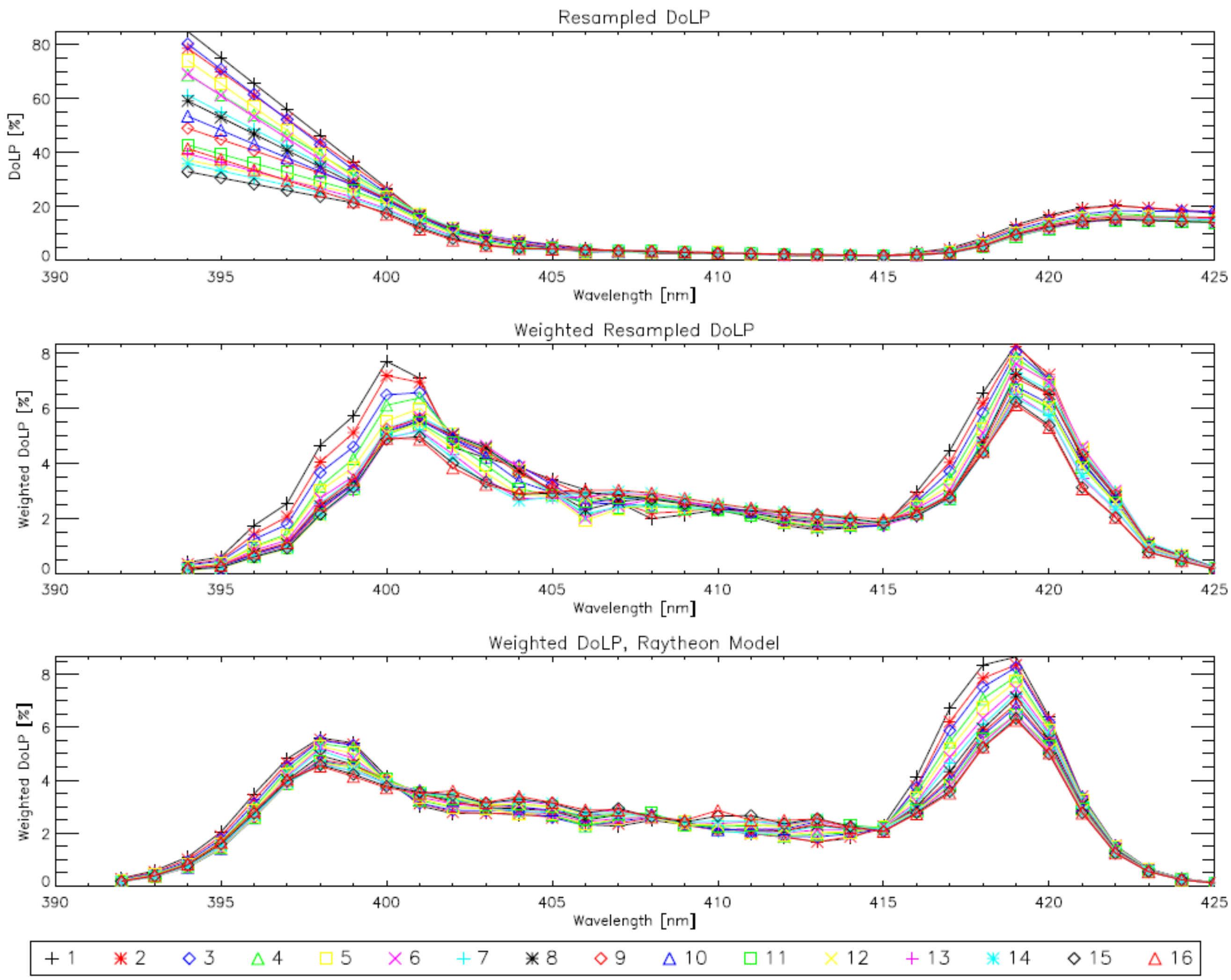

Figure 19: DoLP [%] versus wavelength [nm] for band M1, at +45 degrees scan angle, HAM 1 (unweighted, weighted, and weighted model)

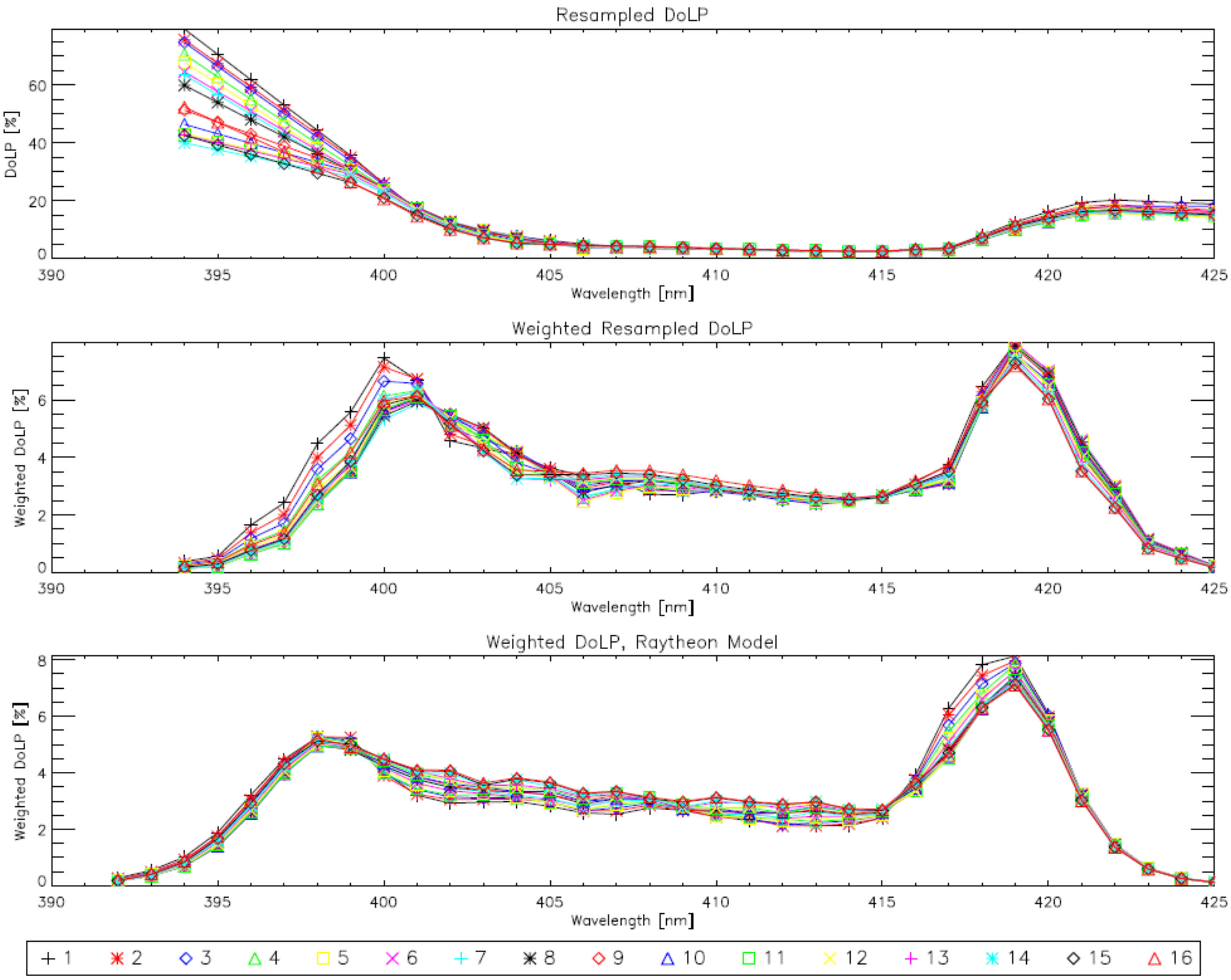

Figure 20: DoLP [%] versus wavelength [nm] for band M4, at -8 degrees scan angle, HAM 1 (unweighted, weighted, and weighted model)

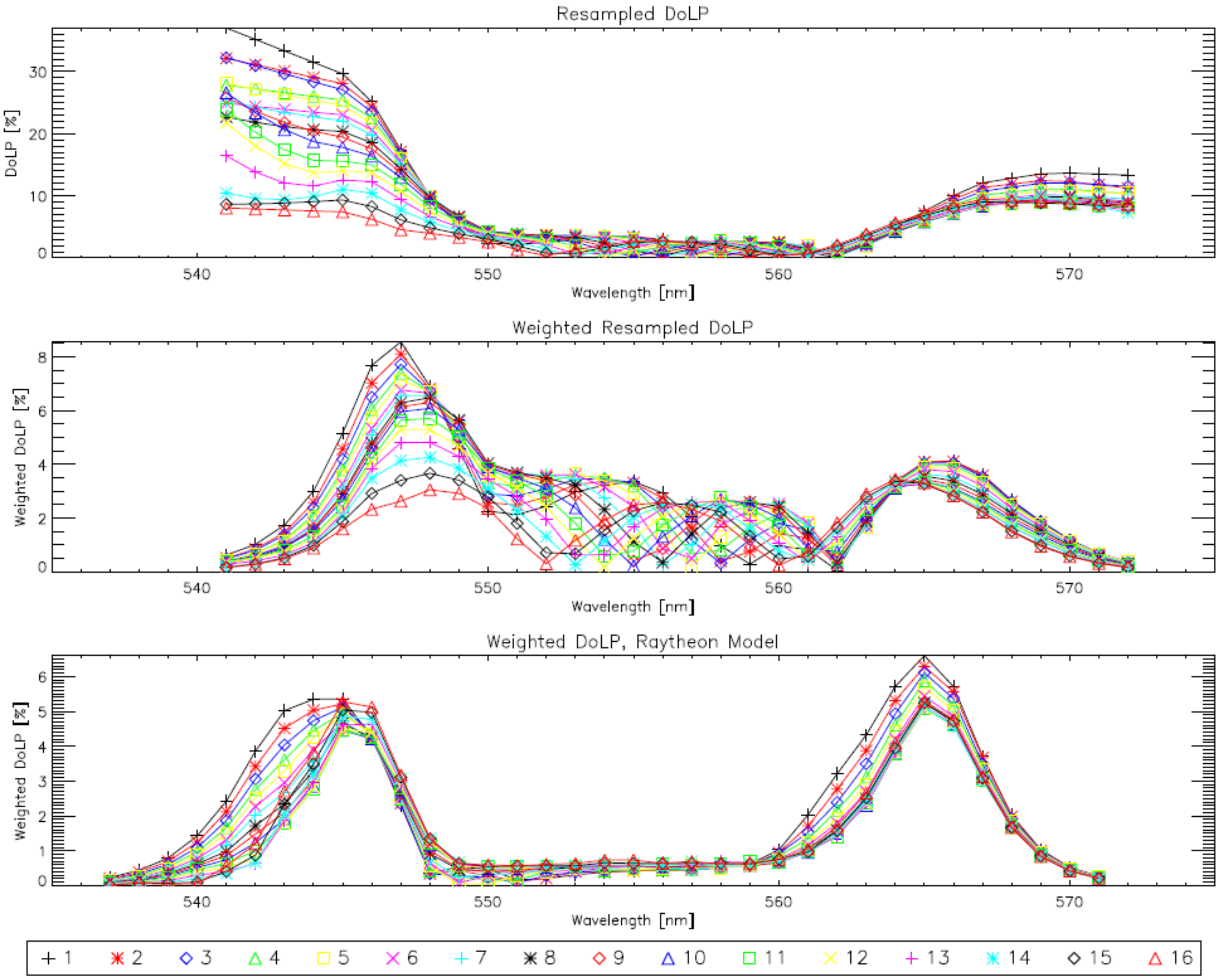

Figure 21: DoLP [%] versus wavelength [nm] for band M4, at -8 degrees scan angle, HAM 0 (unweighted, weighted, and weighted model)

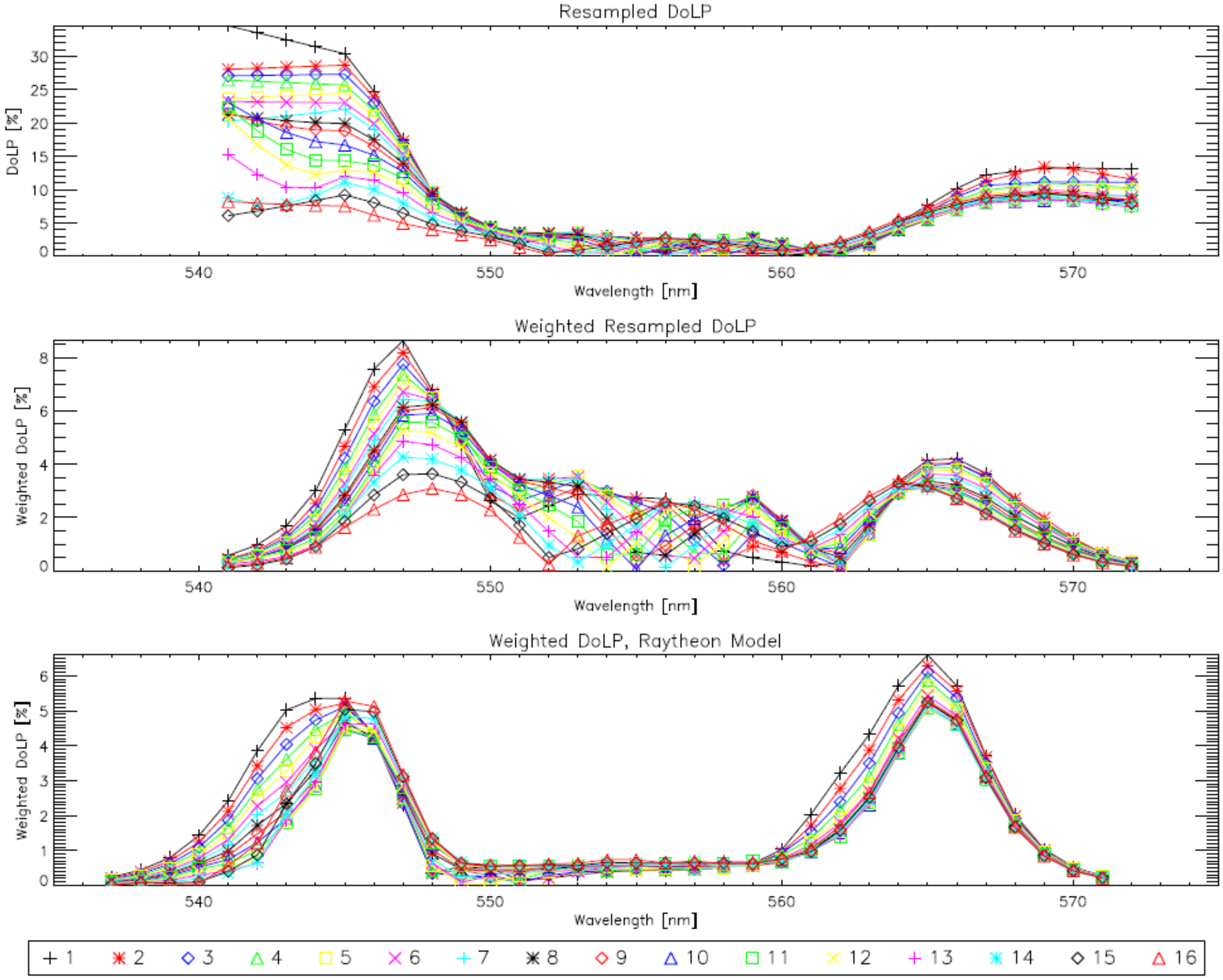

Figure 22: DoLP [%] versus wavelength [nm] for band M4, at +45 degrees scan angle, HAM 1 (unweighted, weighted, and weighted model)

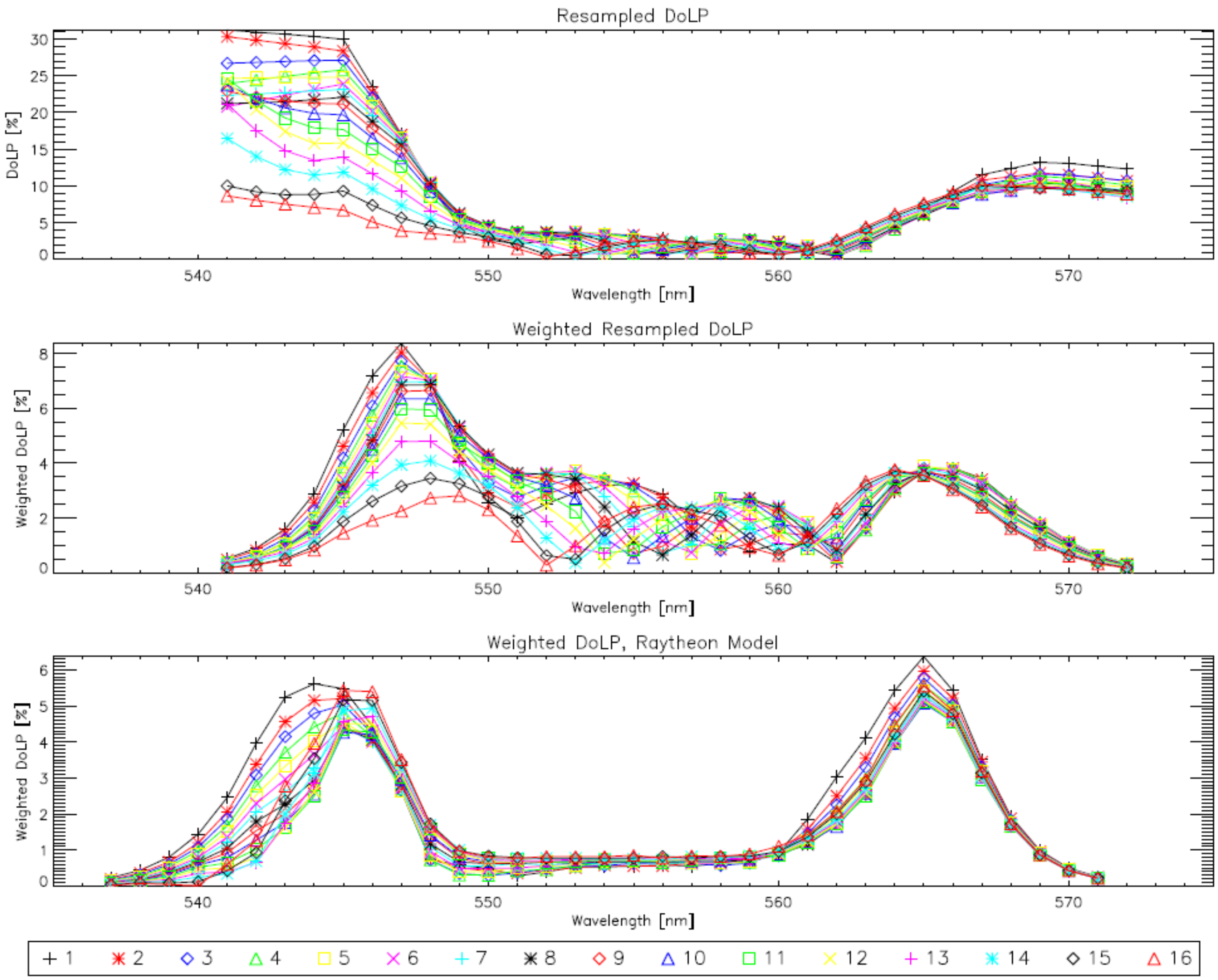

Figure 23: Phase angle [radians] versus wavelength [nm] for band M1, at -8 degrees scan angle, HAM 1 (measured and modeled)

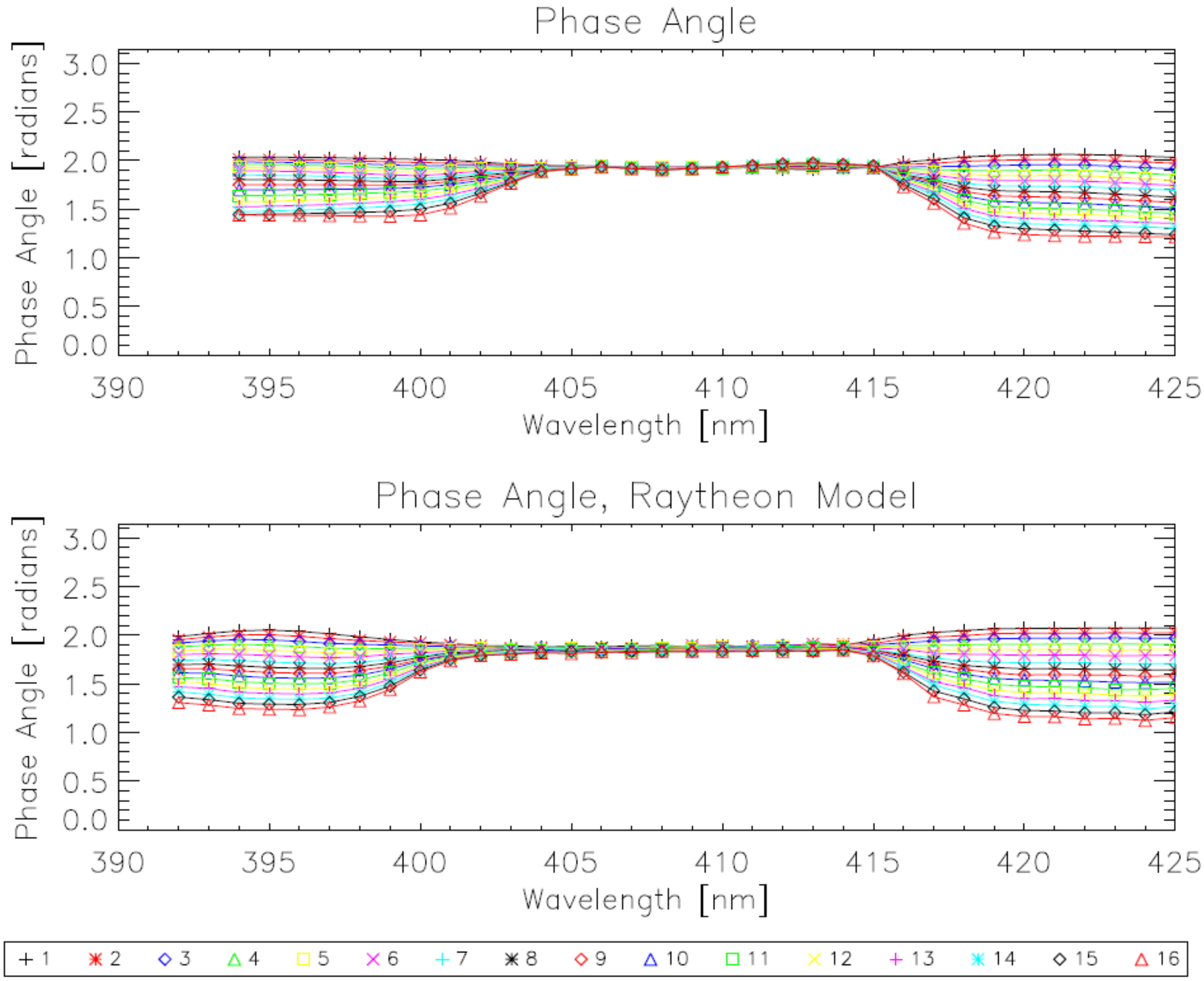

Figure 24: Phase angle [radians] versus wavelength [nm] for band M1, at +45 degrees scan angle, HAM 1 (measured and modeled)

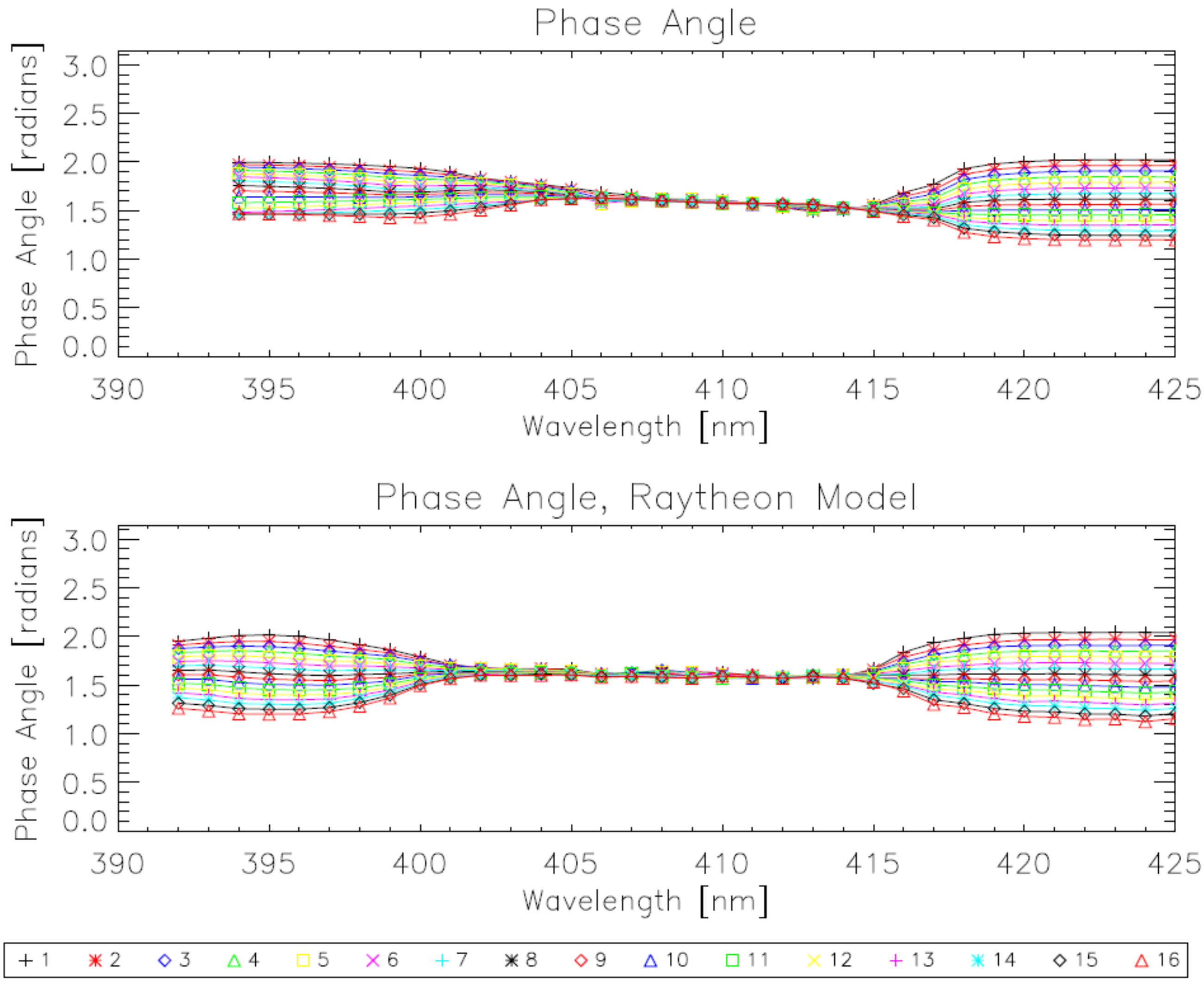

Figure 25: Phase angle [radians] versus wavelength [nm] for band M4, at -8 degrees scan angle, HAM 1 (measured and modeled)

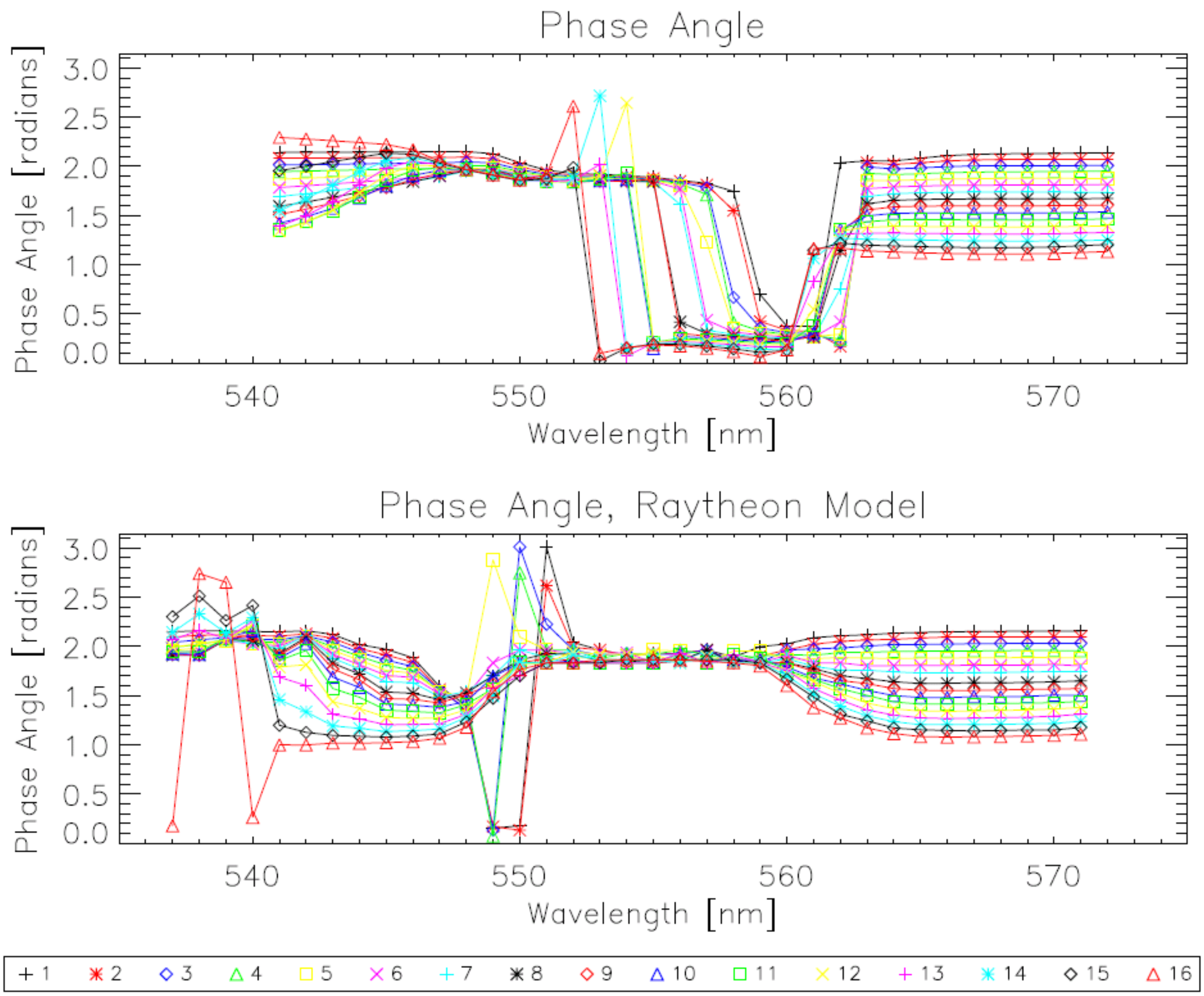

Figure 26: Phase angle [radians] versus wavelength [nm] for band M4, at -8 degrees scan angle, HAM 0 (measured and modeled)

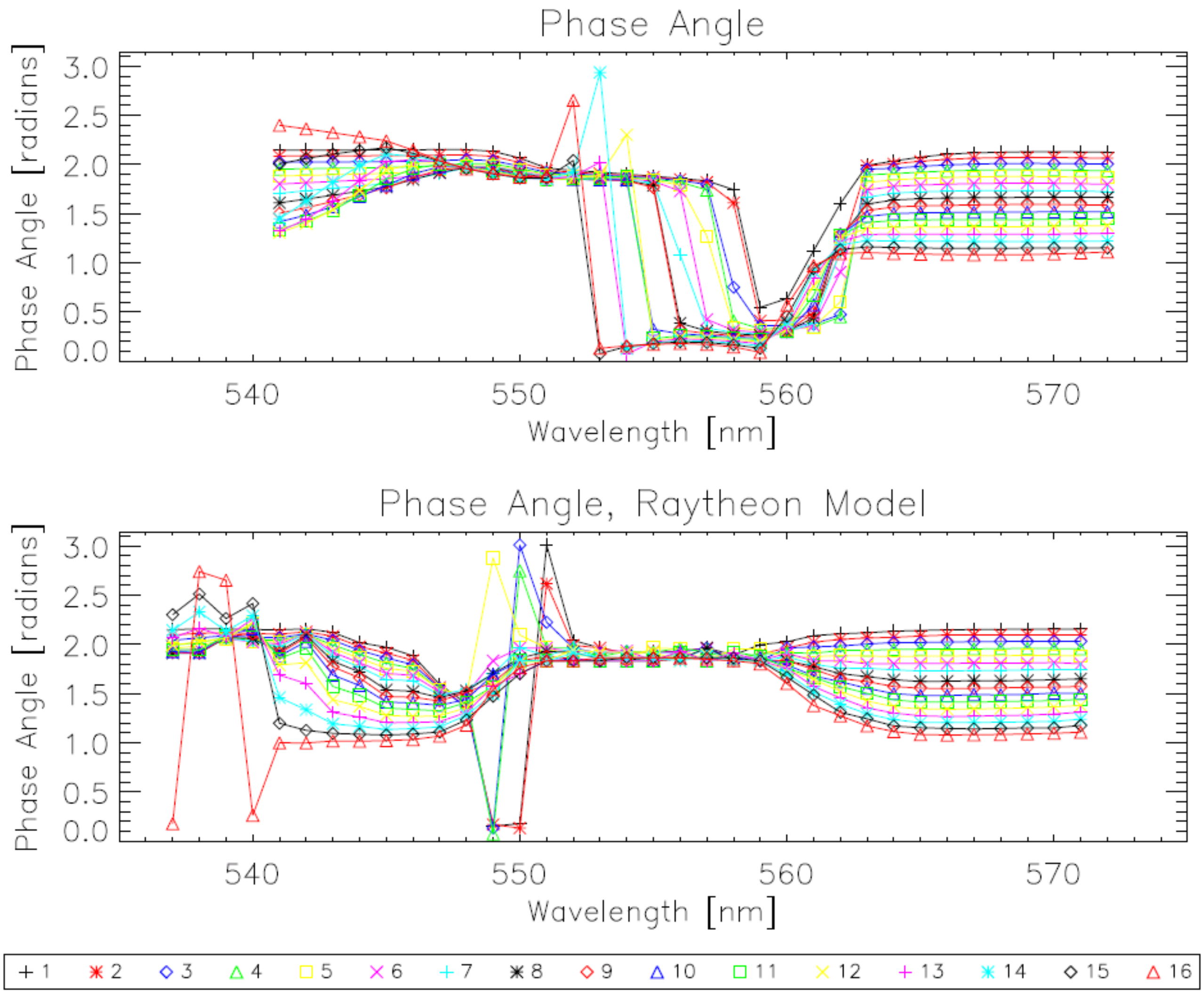

Figure 27: Phase angle [radians] versus wavelength [nm] for band M4, at +45 degrees scan angle, HAM 1 (measured and modeled)

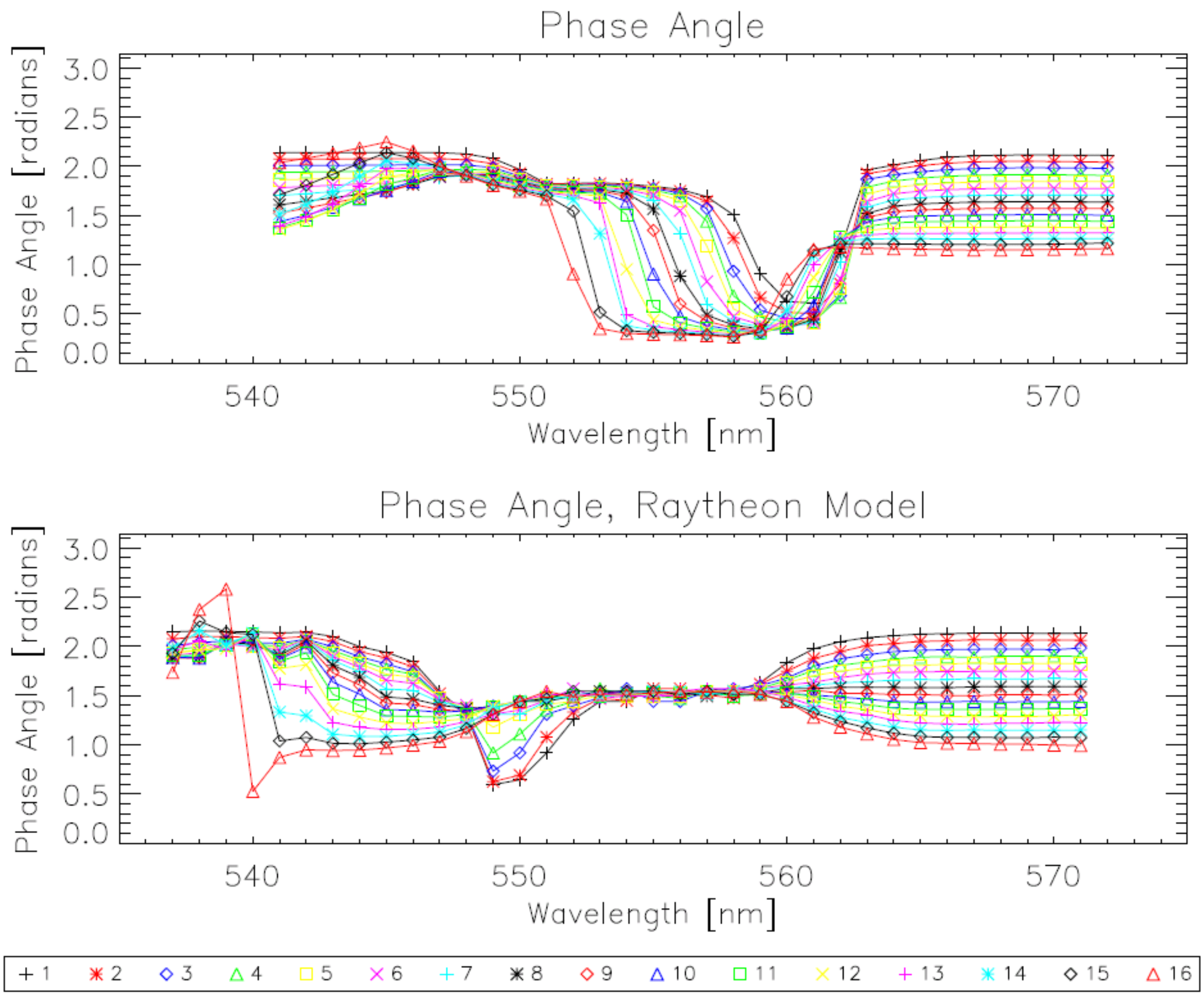

Figure 28: DoLP [%] and phase angle [radians] versus detector for band M1, at -8 degrees scan angle, HAM 1 (measured and modeled)

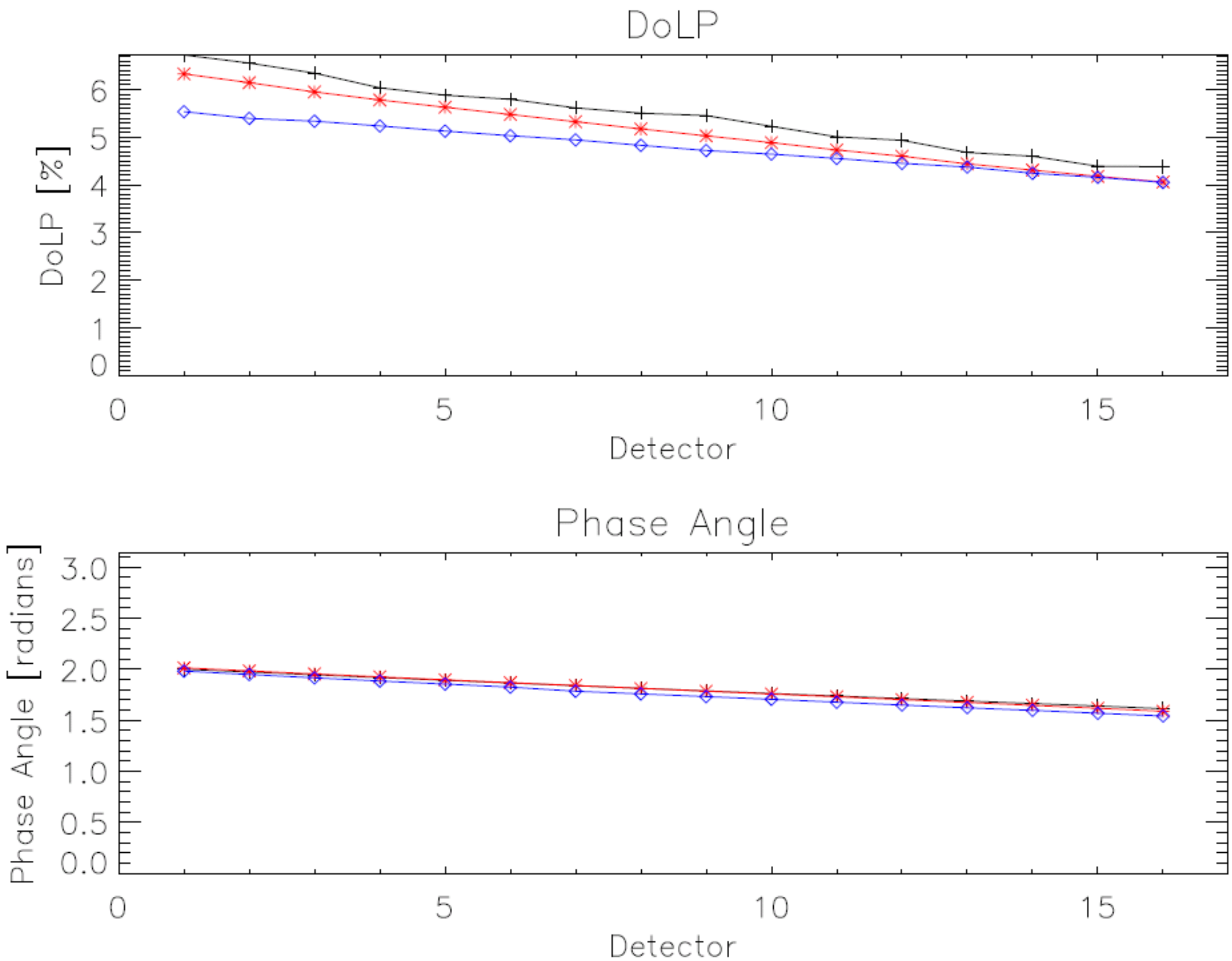

Figure 29: DoLP [%] and phase angle [radians] difference from FP-11 versus detector for band M1, at -8 degrees scan angle, HAM 1 (measured and modeled)

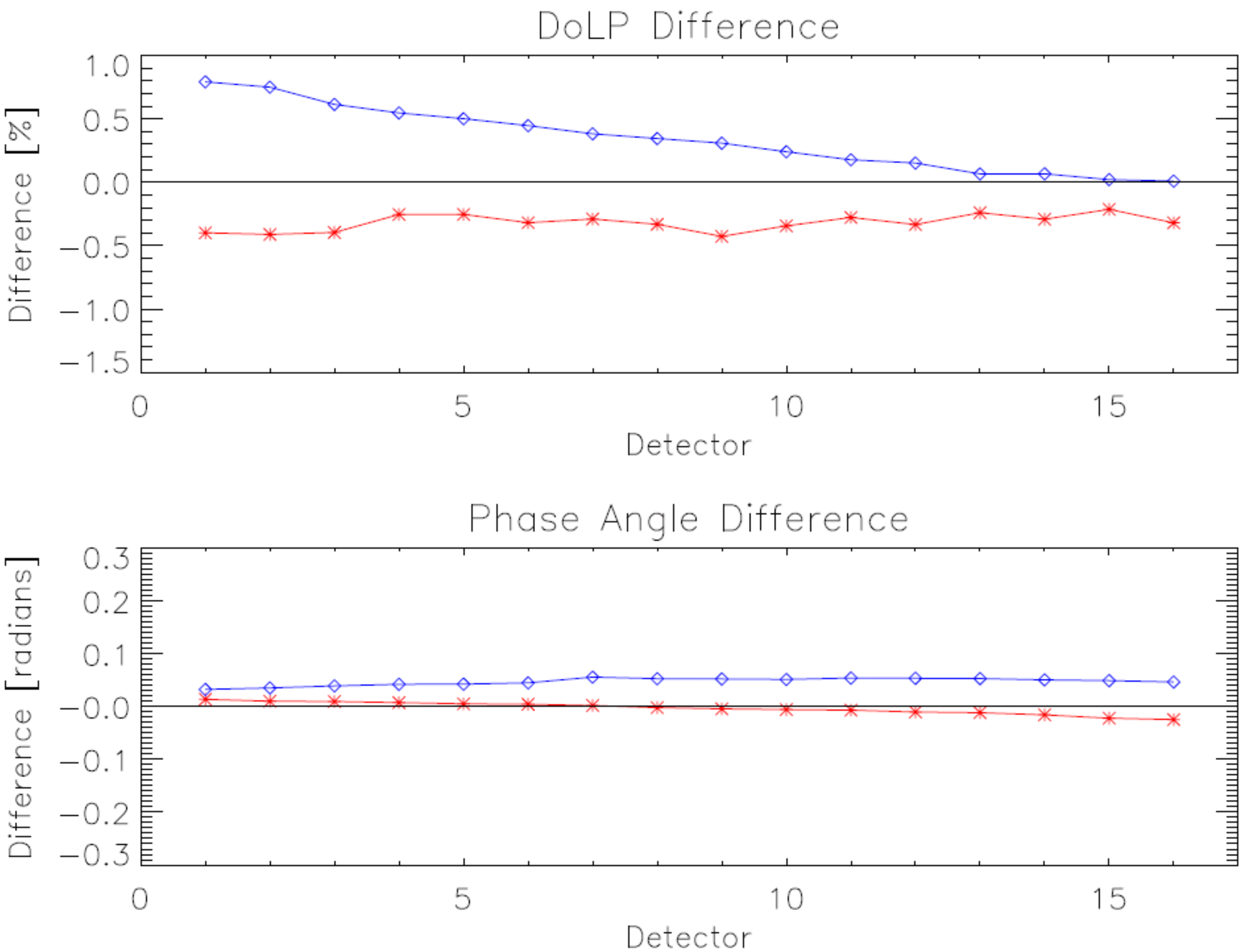

Figure 30: DoLP [%] and phase angle [radians] versus detector for band M1, at +45 degrees scan angle, HAM 1 (measured and modeled)

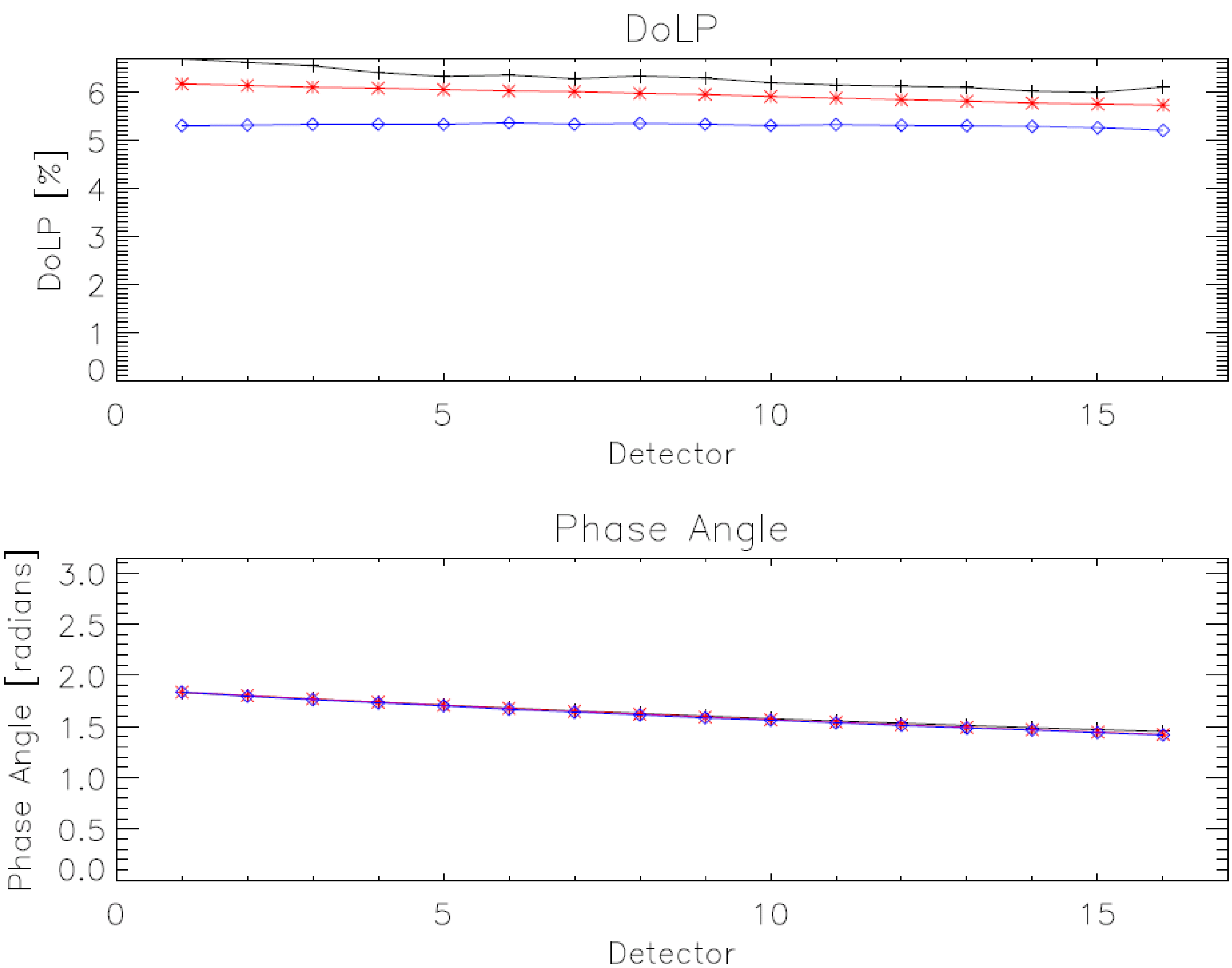

Figure 31: DoLP [%] and phase angle [radians] difference from FP-11 versus detector for band M1, at +45 degrees scan angle, HAM 1 (measured and modeled)

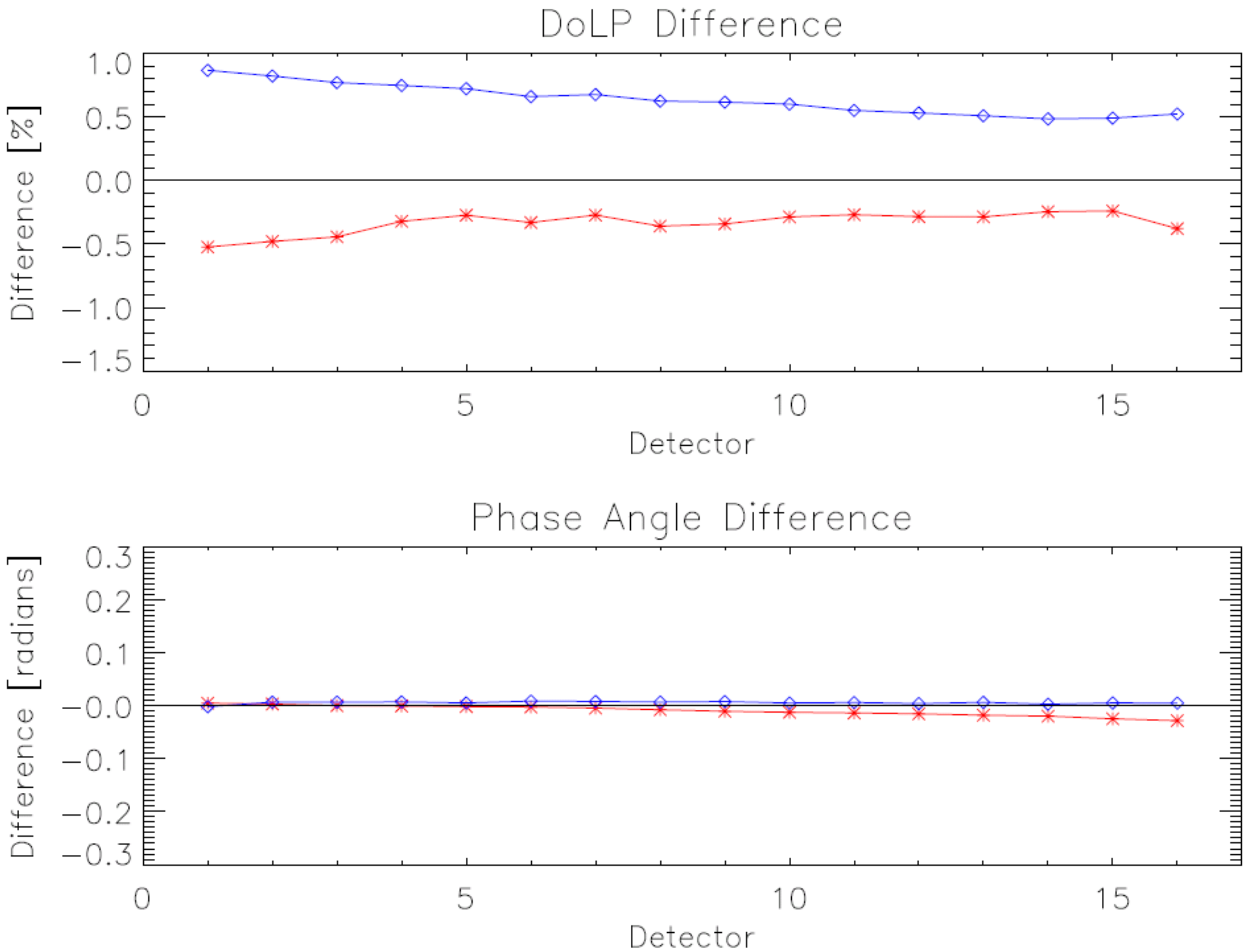

Figure 32: DoLP [%] and phase angle [radians] versus detector for band M4, at -8 degrees scan angle, HAM 1 (measured and modeled)

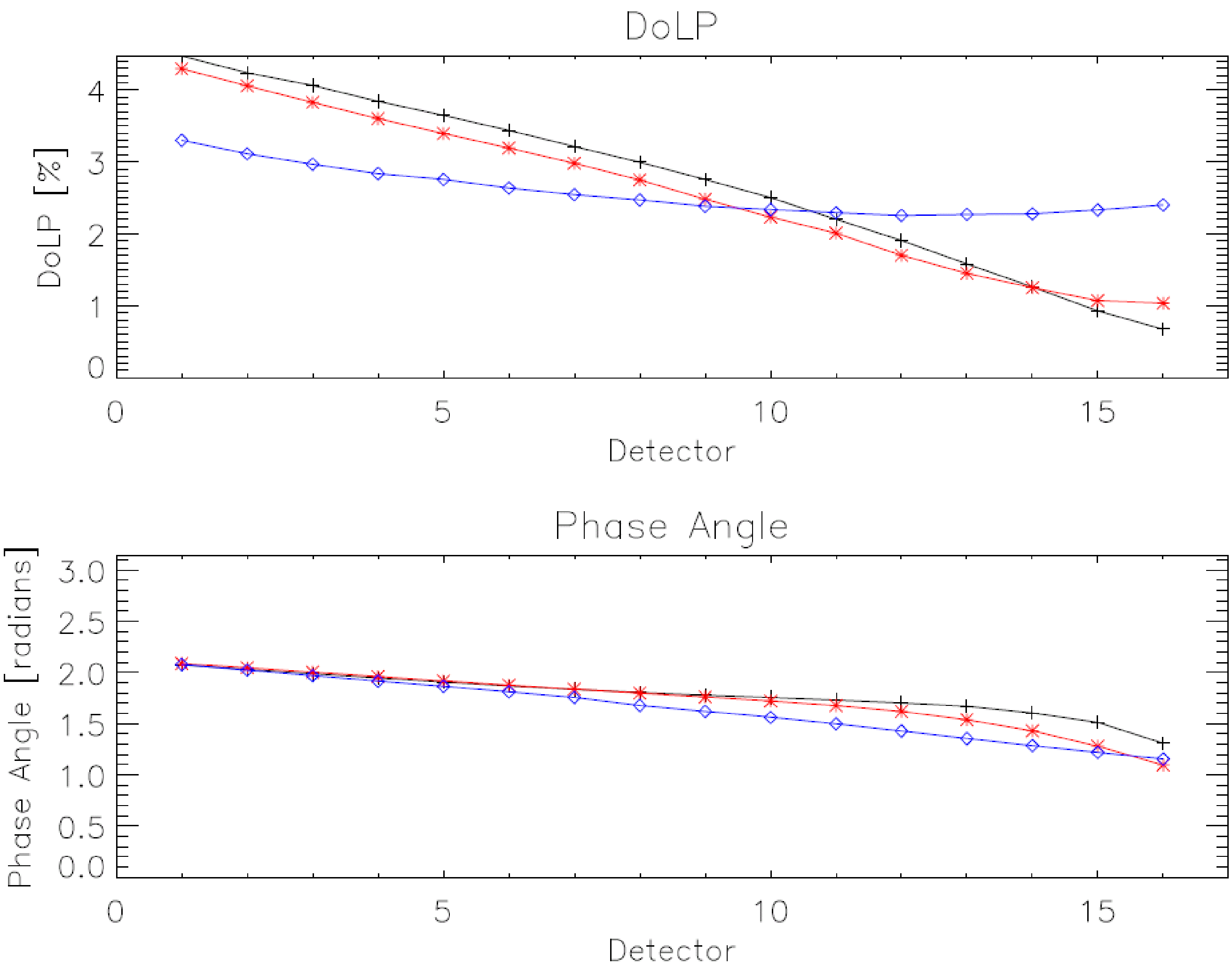

Figure 33: DoLP [%] and phase angle [radians] difference from FP-11 versus detector for band M4, at -8 degrees scan angle, HAM 1 (measured and modeled)

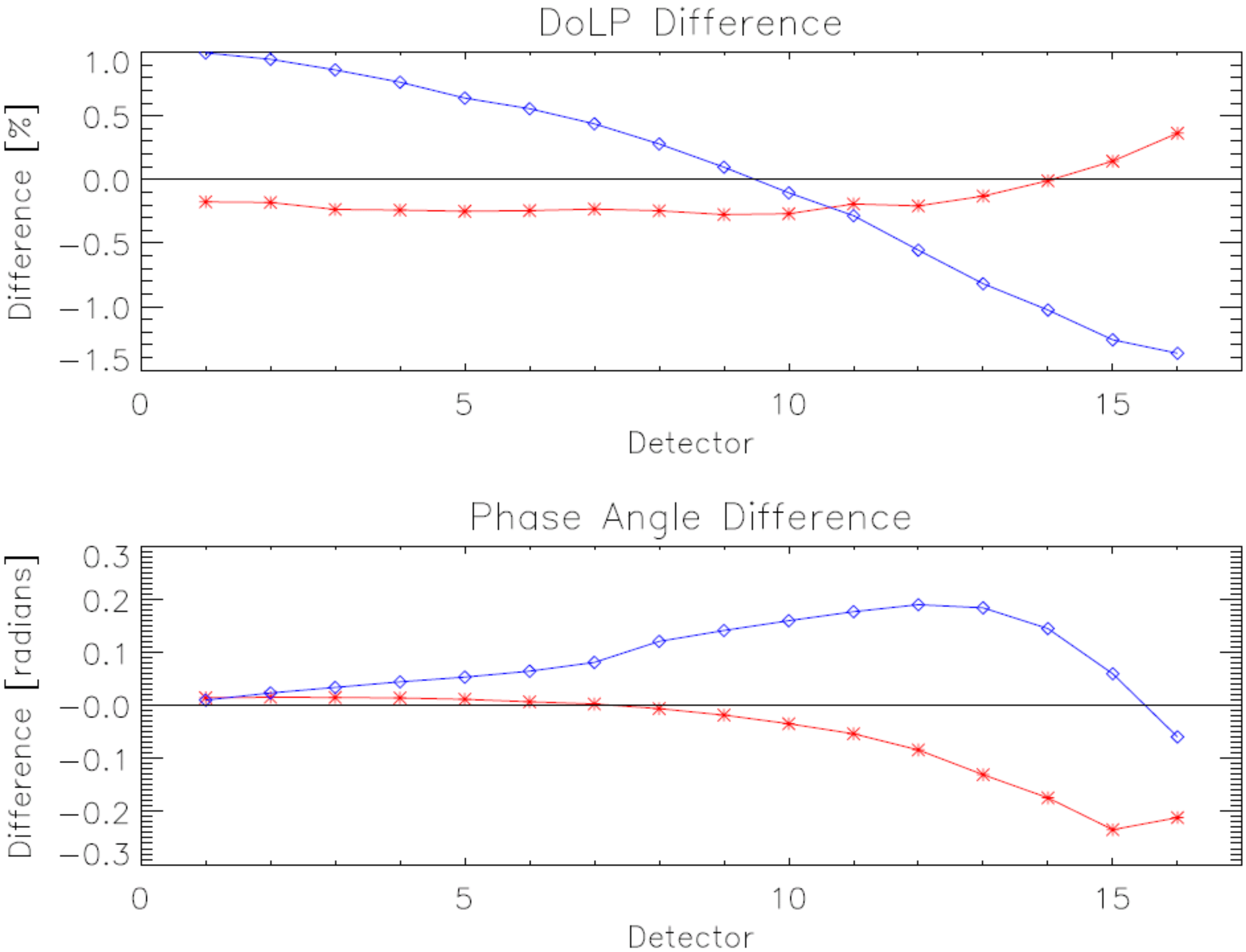

Figure 34: DoLP [%] and phase angle [radians] versus detector for band M4, at -8 degrees scan angle, HAM 0 (measured and modeled)

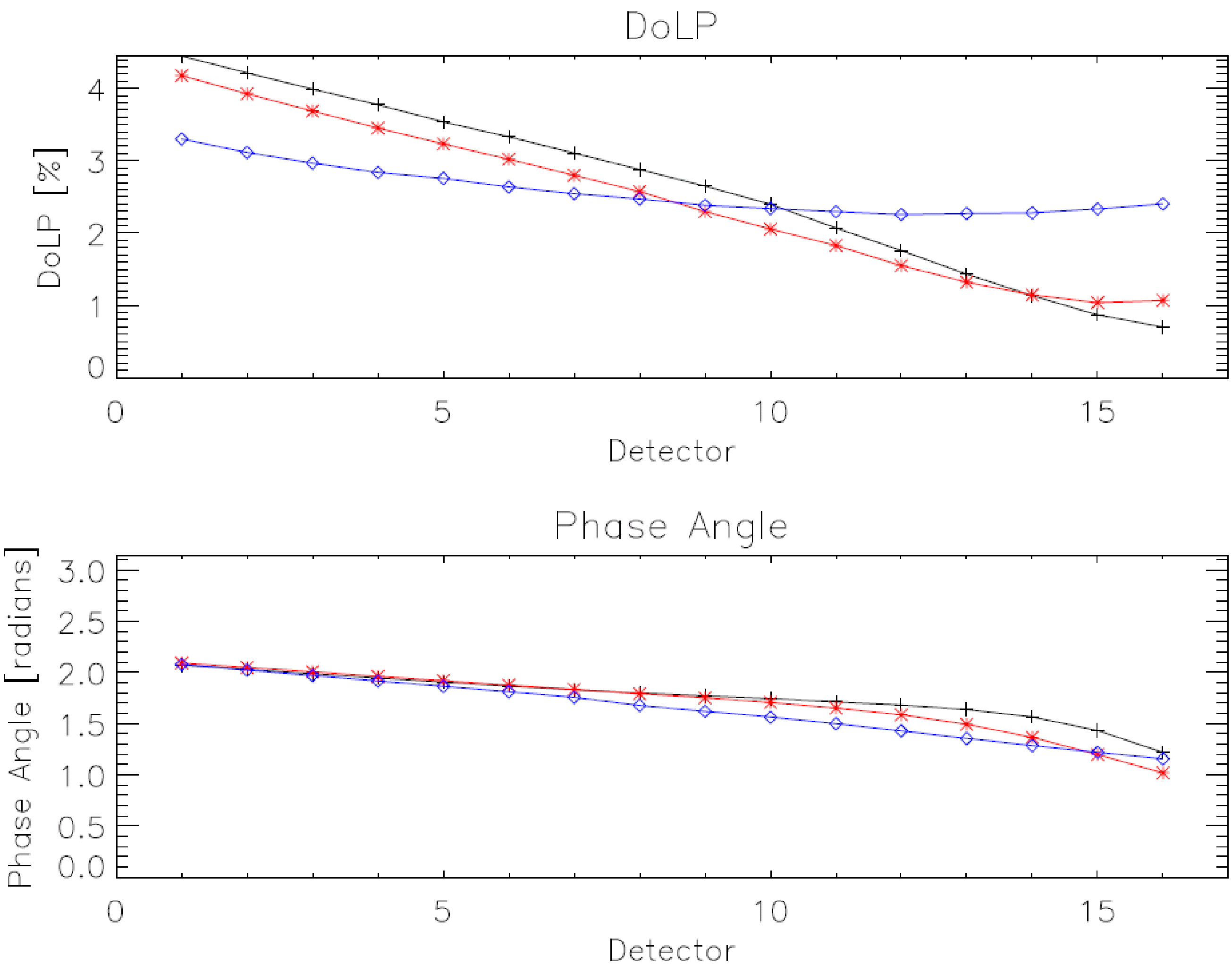

Figure 35: DoLP [%] and phase angle [radians] difference from FP-11 versus detector for band M4, at -8 degrees scan angle, HAM 0 (measured and modeled)

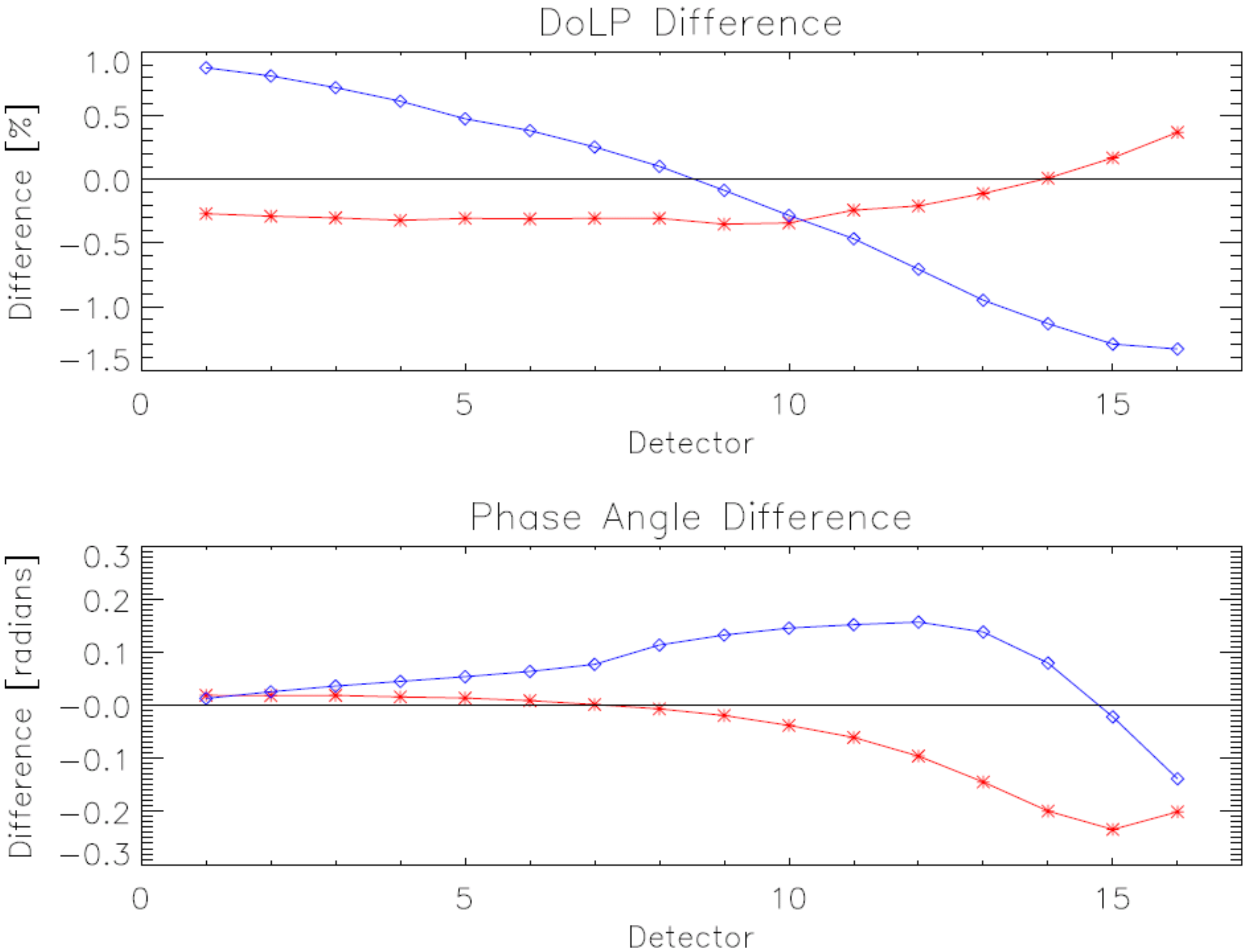

Figure 36: DoLP [%] and phase angle [radians] versus detector for band M4, at +45 degrees scan angle, HAM 1 (measured and modeled)

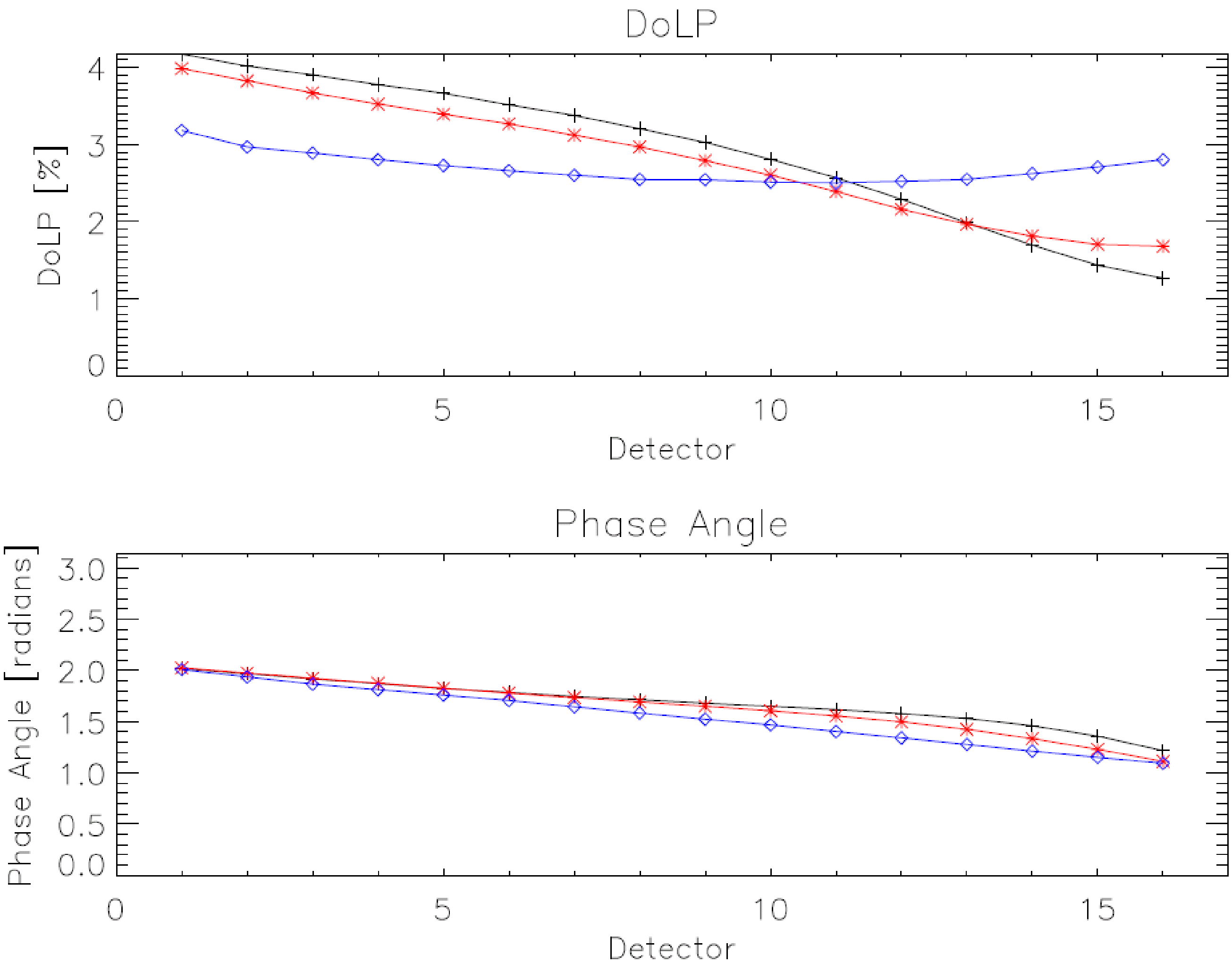

Figure 37: DoLP [%] and phase angle [radians] difference from FP-11 versus detector for band M4, at +45 degrees scan angle, HAM 1 (measured and modeled)